



# Absorption spectra measurements at $\sim 1\text{ cm}^{-1}$ spectral resolution of $^{32}\text{S}$ , $^{33}\text{S}$ , $^{34}\text{S}$ , and $^{36}\text{S}$ sulfur dioxide for the 206–220 nm region and applications to modeling of the isotopic self-shielding

Yoshiaki Endo<sup>1,2\*</sup> , Sebastian O. Danielache<sup>1,3</sup>, Moeko Ogawa<sup>3</sup>, and Yuichiro Ueno<sup>1,2,4</sup> 

<sup>1</sup> Earth-Life Science Institute (WPI-ELSI), Tokyo Institute of Technology, Meguro, Tokyo 152-8550, Japan

<sup>2</sup> Department of Earth and Planetary Sciences, Tokyo Institute of Technology, Meguro, Tokyo 152-8551, Japan

<sup>3</sup> Faculty of Science & Technology, Sophia University, Chiyoda-ku, Tokyo 102-8554, Japan

<sup>4</sup> Japan Agency for Marine-Earth Science and Technology (JAMSTEC), Natsushima-cho, Yokosuka 237-0061, Japan

\* Corresponding author E-mail: endo.y.ac@m.titech.ac.jp

## Abstract

The sulfur isotope fractionation that occurs during  $\text{SO}_2$  photolysis is key to explaining the isotope signatures stored in ancient sedimentary rocks and understanding the atmospheric compositions of the early Earth and early Mars. Here, we report the photoabsorption cross-sections of  $^{32}\text{SO}_2$ ,  $^{33}\text{SO}_2$ ,  $^{34}\text{SO}_2$ , and  $^{36}\text{SO}_2$  measured from 206 to 220 nm at 296 K. The wavelength resolution was set to  $1\text{ cm}^{-1}$ , 25 times higher than that of previous  $\text{SO}_2$  isotopologue absorption spectra measurements. The precision of  $\sim 10\%$  is in agreement with previously reported  $\text{SO}_2$  absorption spectra. In comparison with previously reported high-resolution spectra of natural abundance,  $\text{SO}_2$  measurements demonstrate smaller cross-sectional magnitudes at absorption peaks and an offset wavelength by  $\sim 0.016\text{ nm}$ . Using the newly recorded isotopologue spectra, we calculated the sulfur isotope fractionation for self-shielding during  $\text{SO}_2$  photolysis. The calculated  $^{34}\text{S}$  fractionation ( $^{34}\varepsilon$ ) roughly reproduces the observed relationship between  $^{34}\varepsilon$  and the  $\text{SO}_2$  column density in previous photolysis experiments. Thus, the cross-section is useful for predicting  $^{34}\text{S}/^{32}\text{S}$  isotope fractionation in an optically thick  $\text{SO}_2$  atmosphere. In contrast, for mass-independent fractionation (MIF-S, i.e., non-zero  $\Delta^{33}\text{S}$ ), the measured spectra predicted a weakly negative  $\Delta^{33}\text{S}/\delta^{34}\text{S}$  slope of about  $-0.1$ . The small  $\Delta^{33}\text{S}/\delta^{34}\text{S}$  slope is consistent with the slopes of  $\text{SO}_2$  photolysis experiments under high-pressure atmospheres (i.e., the pressure broadened absorption line width will be comparable to the spectral resolution). Therefore, MIF-S during photolysis experiments was linked to spectroscopic measurements for the first time. We conclude that reasonable precision and high-resolution spectroscopic measurements are key to explaining the origin of MIF-S at column densities below  $10^{18}\text{ cm}^{-2}$ . However, MIF-S production in chamber experiments or atmospheric conditions may require understanding pressure or temperature effects, such as linewidth broadening on the UV-absorption spectra, and how these effects manifest themselves on isotopologues.

**Keywords** Sulfur dioxide, Sulfur isotopes, Mass-independent fractionation, Self-shielding, Early Earth atmosphere

**Dates** Received: June 18, 2021 Accepted: October 20, 2021 Advance publication: December 8, 2021



## Introduction

Sulfur dioxide ( $\text{SO}_2$ ) plays an important role in planetary atmospheres, including that of the Earth. This gas has been released into the atmosphere by volcanic activity throughout Earth's history (Holland, 2002; Gaillard *et al.*, 2011; Olson *et al.*, 2019; Ohmoto, 2020), is a candidate greenhouse gas in early Mars (Halevy *et al.*, 2007; Johnson *et al.*, 2008), and has also been observed in Venus and Io's atmospheres (e.g., Vandaele *et al.*, 2017; Feaga *et al.*, 2009).

$\text{SO}_2$  has two strong structured absorption bands in the UV region; therefore, UV radiation triggers complex photochemical processes in this molecule (e.g., Heicklen *et al.*, 1980). The 165–230 nm absorption band occurs where  $\text{SO}_2$  is photolyzed by wavelengths below 218.7 nm (Katagiri *et al.*, 1997) by its excitation to the  $\text{C}^1\text{B}_2$  state. The second absorption band occurs in the 250–340 nm region, where  $\text{SO}_2$  is excited to the  $\text{B}(\text{B}_1 + \text{A}_2)$  state. In the oxygen-free and ozone-free atmosphere of the early Earth, photons above approximately 190 nm penetrated the troposphere (Ueno *et al.*, 2009), making complex light-induced chemistry possible for this molecule.

$\text{SO}_2$  photolysis originates large mass-independent fractionation of sulfur isotopes (MIF-S), which is notably distinct from the more commonly observed mass-dependent fractionation (e.g., Farquhar *et al.*, 2001; Whitehill and Ono, 2012; Franz *et al.*, 2013; Ono, 2017). Specifically, MIF-S has been found in Archean sedimentary rocks (e.g., Farquhar *et al.*, 2000a), Martian meteorites (e.g., Farquhar *et al.*, 2000b), sulfate aerosols in polar ice (e.g., Savarino *et al.*, 2003), and in the present atmosphere (e.g., Romero and Thiemens, 2003). The Archean MIF-S may provide insights into the atmospheric chemical composition at that time (e.g., Ono, 2017). Previous laboratory experiments and numerical modeling suggest that MIF-S reflects various atmospheric parameters: very low partial pressure (<2 ppm) of  $\text{O}_2$  is required to preserve the MIF-S signatures ( $\Delta^{33}\text{S} \neq 0$ ) in both sulfide and sulfate minerals (Pavlov and Kasting, 2002; Zahnle *et al.*, 2006);  $\text{SO}_2$  column density (or partial pressure of  $\text{SO}_2$ ) changes  $\Delta^{33}\text{S}$  and  $\Delta^{36}\text{S}$  magnitudes (Ono *et al.*, 2013); atmospheric pressure changes  $\Delta^{36}\text{S}/\Delta^{33}\text{S}$  slope (Lyons *et al.*, 2018; Endo *et al.*, 2019); reducing gases such as hydrocarbons and carbon monoxide (CO) changes the  $\Delta^{36}\text{S}/\Delta^{33}\text{S}$  slope by MIF-S in  $\text{SO}_2$ -photoexcitation chemistry (Whitehill *et al.*, 2013; Endo *et al.*, 2016; Kroll *et al.*, 2018); and strong UV absorption, such as by organic haze, changes the branching ratios of  $\text{SO}_2$  photolysis/photoexcitation and MIF-S (Zerkle *et al.*, 2012). In addition, the polymerization of elemental sulfur, excluding  $\text{SO}_2$  photochemistry, has also been proposed as an MIF-S mechanism (Babikov, 2017; Harman *et al.*, 2018; Lin and Thiemens, 2020).

The most common feature of the Archean geologic

MIF-S is a  $\Delta^{36}\text{S}/\Delta^{33}\text{S}$ -slope of  $\sim -0.9$  (Farquhar *et al.*, 2000a). Recently, Endo *et al.* (2016) and Mishima *et al.* (2017) argued that this can be explained by mixing MIF-S during  $\text{SO}_2$  photolysis ( $\Delta^{36}\text{S}/\Delta^{33}\text{S} \sim -2.4$ ) with MIF-S induced during  $\text{SO}_2$  photoexcitation ( $\Delta^{36}\text{S}/\Delta^{33}\text{S} \sim +0.8$ ). A highly reducing atmosphere, such as Earth's ancient atmosphere containing a significant percentage of carbon monoxide or methane, is required to propagate MIF-S induced by  $\text{SO}_2$  photoexcitation. Independently, a highly reducing atmosphere is also speculated based on xenon isotopes (Avice *et al.*, 2018; Zahnle *et al.*, 2019). However, the second most basic trend,  $\Delta^{33}\text{S}/\delta^{34}\text{S}$  ( $\sim +0.9$ ; Ono *et al.*, 2009), cannot be explained. The mechanisms underlying MIF-S still require further exploration.

In the present study, we focused on MIF-S during  $\text{SO}_2$  photolysis, although  $\text{SO}_2$  photoexcitation also causes a large MIF-S (Whitehill *et al.*, 2013). The underlying mechanisms of MIF-S in the photoexcitation are likely isotopologue-specific perturbations (Whitehill *et al.*, 2013), and the mechanisms may also occur in isotope fractionation during  $\text{N}_2$  and  $\text{CO}$  photolysis (Chakraborty *et al.*, 2008, 2014). The MIF-S during  $\text{SO}_2$  photolysis is dependent on the  $\text{SO}_2$  column density and total pressure. This relationship can be explained by decreasing  ${}^{32}\text{SO}_2$  (and possibly  ${}^{33}\text{SO}_2$  at high pressure, i.e., significant pressure broadening in  $\text{SO}_2$  absorption lines) photolysis rates due to  $\text{SO}_2$  own absorption. This process is known as self-shielding or isotopic self-shielding (Ono *et al.*, 2013; Lyons *et al.*, 2018; Endo *et al.*, 2019). The nature of self-shielding was recently summarized and reviewed by Lyons (2020) and Thiemens and Lin (2021). Isotope fractionation in photolysis is predicted by the absorption cross-sections of isotopologues (Miller and Yung, 2000). A small MIF-S was predicted for optically thin  $\text{SO}_2$  (i.e., without self-shielding) based on high-precision and low-wavelength resolution  ${}^{32}\text{SO}_2$ ,  ${}^{33}\text{SO}_2$ ,  ${}^{34}\text{SO}_2$ , and  ${}^{36}\text{SO}_2$  (hereafter  ${}^{32,33,34,36}\text{SO}_2$ ) absorption spectra (Endo *et al.*, 2015; Izon *et al.*, 2017); this was consistent with the results of  $\text{SO}_2$ -photolysis experiments (Endo *et al.*, 2016). In principle, a large MIF-S at optically thick  $\text{SO}_2$  (i.e., with self-shielding) can also be predicted; however, predictions by absorption measurements for cross-sections of  $\text{SO}_2$  isotopologues did not match the MIF-S observed using  $\text{SO}_2$ -photolysis experiments (Ono *et al.*, 2013). This discrepancy is likely caused by the complex ro-vibrational structures of  $\text{SO}_2$ -absorption spectra and the insufficient wavelength resolutions of spectroscopic measurements.

In this study, we report reasonable precision and high-resolution measurements of UV-absorption spectra of  ${}^{32,33,34,36}\text{SO}_2$  isotopologues using isotope enrichment samples. The experimental device used in this report was a full-vacuum fast Fourier transform (FFT) spectrometer with a wavelength resolution of  $1 \text{ cm}^{-1}$ . This was  $\sim 25$  times higher than that in previous reports of  $\text{SO}_2$  isotopo-

logues (Danielache *et al.*, 2008; Endo *et al.*, 2015), and ~8 times lower than that reported by a previous study that used the highest resolution to measure the natural abundance of SO<sub>2</sub> (Stark *et al.*, 1999). Due to the trade-off between resolution and precision, the precision used was ~10 times lower than that of previous studies using a dual-beam monochromator to attain high-precision measurements (Endo *et al.*, 2015). Absorption spectra were measured from 206 to 220 nm with sufficient precision, although most of the SO<sub>2</sub> was photolyzed by photons from 190 to 220 nm in the Archean atmosphere. Although uncertainty remains as a result of this, the fractionation factors predicted by this study are comparable with isotope compositions of products used in previous SO<sub>2</sub>-photolysis experiments at optically thick SO<sub>2</sub> conditions in which self-shielding occurs. In addition, we compared the results with a simple analytical self-shielding model for the Archean MIF-S. This simple model allowed us to predict the large enrichment or depletion of clumped isotope signatures caused by self-shielding. In sum, we attempted to link sulfur isotope fractionations during photolysis experiments to spectroscopic measurements and discuss the Archean MIF-S trend produced by self-shielding.

## Methods

### Experimental samples

The samples measured in this report were previously presented and described in detail by Danielache *et al.* (2012). To ensure the isotopic purity of the samples, CuO and elemental <sup>32</sup>S, <sup>33</sup>S, <sup>34</sup>S, and <sup>36</sup>S sealed in a quartz tube under vacuum were heated at 950°C for 15 min. The resultant <sup>32,33,34,36</sup>SO<sub>2</sub> gas and unreacted O<sub>2</sub> were separated using freeze-pump-thaw cycling and further purified using gas chromatography. The stability of the samples during long storage periods was maintained using sealed preheated Pyrex tubes, and the tubes were stored in a dark environment. During the experiments, when samples were used on a daily basis, containers consisting of stainless steel (SUS316) tubing welded to a bellows-sealed valve (SS-4H-TH3, Swagelok Company, U.S.A.) were used.

### Spectrometry and measurements

The absorption cross-sections were determined using an FFT spectrometer (VERTEX80v, Bruker Inc., U.S.A.) equipped with a deuterium lamp (L6301-50, Hamamatsu Photonics K.K., Japan), a 10.0-cm long cell with UV-grade LiF windows, and a VUV-diode detector and calcium fluoride beam splitter. The inside of the spectrometer was constantly evacuated by a dry pump, and the interferometer was operated under a constant nitrogen gas flow. The wavelength scale of this study was calibrated using a He–Ne laser (15,798 cm<sup>-1</sup>) and water

absorption lines (1554.353 and 7306.74 cm<sup>-1</sup>). Under these experimental conditions, a spectral resolution of 1 cm<sup>-1</sup> yielded signal-to-noise ratios (SNRs) of ~20 and ~100 at 206 and 220 nm, respectively.

The SO<sub>2</sub> cross-section is known to vary more than one order of magnitude within the measured wavelength range. To maximize the SNR conditions for all wavelengths, the sample gas pressures were set between 15 and 300 Pa by diffusion in a vacuum line. Pressures were measured using two capacitance manometers (CMR362, 0.01–110 Pa range and CMR364, 1–1.1 × 10<sup>4</sup> Pa range; Pfeiffer Vacuum GmbH, Germany). The resolution and accuracy of both manometers were 0.003 and 0.2% at full scale and reading, respectively. Inaccuracies in pressure measurements induce an uncertainty of approximately ≤0.5% of the estimated cross-section. The measurements took approximately 15 min, and during this process, the sample gas pressure gradually decreased (maximum 0.3 Pa), potentially due to adsorption to the gas cell and the stainless steel vacuum line. The sample pressure utilized was the average of the pressures before and after the measurement. We assigned a conservative maximum uncertainty of 1% from the pressure.

The absorption spectrum was obtained from photon intensity spectra of the empty cell and sample. The photon intensity spectra were calculated from 100 interferograms at a resolution of 1 cm<sup>-1</sup>. A Blackman–Harris three-term apodization function, a Fourier transform window from 0 to 60,000 cm<sup>-1</sup>, and a zero-filling factor of 2 were used to produce a spectrum with an energy range of 54,000 to 35,000 cm<sup>-1</sup> with a data point spacing of 0.241085 cm<sup>-1</sup>. Background intensity spectra ( $I_{\text{vacuum}}$ ) and gas sample spectra ( $I_{\text{sample}}$ ) were measured in an alternating fashion.

The amplitude drift of the signal can be assessed by comparing the two background spectra. The average signal drift between 206 and 220 nm was calculated to be ~15%. A moving average of 41 points was introduced to reduce noise in the background spectra. In contrast, no such smoothing procedure was implemented for the sample spectra ( $I_{\text{sample}}$ ).

In our previous reports (Danielache *et al.*, 2008, 2012), the background spectra at the time of the measurement were taken as the average spectra of the empty cell before ( $I_{\text{vacuum-before}}$ ) and after ( $I_{\text{vacuum-after}}$ ) recording the sample spectra. This approach partially corrects the drift effects on the background spectrum. In this study, a more realistic approach was used to reduce uncertainties induced by drift effects. Since SO<sub>2</sub> spectra in the energy range of 235 to 245 nm have very weak absorption cross-sections that are more than one order of magnitude smaller ( $6 \times 10^{-20}$  cm<sup>2</sup>; Rufus *et al.*, 2003, at transmittance above 0.96) than the spectra involved in the photolysis process, which is far beyond the photolysis threshold (219.2 nm; Okabe, 1971), the background

spectrum was calculated by minimizing  $x$  for the following relationship:

$$\sum [x|I_{\text{vacuum-before}}(\lambda) - I_{\text{sample}}(\lambda)| + (1-x)|I_{\text{vacuum-after}}(\lambda) - I_{\text{sample}}(\lambda)|] \quad (1)$$

where the summation expands over the 235–245-nm energy range.  $x$  was selected from 0.0, 0.1, ..., 1.0. Once  $x$  was obtained, the corrected background spectrum ( $I_{\text{vacuum}}'(\lambda)$ ) was calculated as:

$$I_{\text{vacuum}}'(\lambda) = x I_{\text{vacuum-before}}(\lambda) + (1-x) I_{\text{vacuum-after}}(\lambda) \quad (1')$$

This correction to the spectral drift from the UV source produces a difference ranging from 1% to 4.5%. Additionally, even when the deuterium lamp was turned off, the recorded intensities were not zero ( $I_{\text{dark}}$ ), indicating that the intensities include a signal that arises from the UV (such as electronics or stray light). To correct for this error, the averaged intensities from 200 to 220 nm were subtracted from  $I_{\text{vacuum}}'(\lambda)$  and  $I_{\text{sample}}$  and defined as:

$$I_{\text{vacuum}}'' = I_{\text{vacuum}}' - I_{\text{dark-average}}$$

$$I_{\text{sample}}' = I_{\text{sample}} - I_{\text{dark-average}}$$

The plots describing these calibrations are summarized in Fig. S1.  $I_{\text{dark-average}}$  and  $I_{\text{dark-stdev}}$  were calculated using the averaged intensities between 200 and 220 nm under no-light conditions, and resulting data that satisfied the following conditions were excluded:

$$1) I_{\text{sample}} < 2I_{\text{dark-average}} + 2I_{\text{dark-stdev}}$$

$$2) I_{\text{vacuum}}' - I_{\text{sample}} < 2I_{\text{dark-stdev}}.$$

By imposing these strict filters, instances with low SN ratios were not included in the final spectra.

Absorption cross-sections were calculated by the Beer's law:

$$\sigma = A/\rho \quad (2)$$

where  $\sigma$  is the absorption cross-section ( $\text{cm}^2$ ),  $\rho$  is the column density of the sample gas (calculated by the ideal gas law in  $\text{cm}^{-2}$ ), and  $A$  is the absorbance, defined as

$$A = \ln(I_{\text{vacuum}}''/I_{\text{sample}}') \quad (3)$$

Because the wavelength resolution is not sufficient to resolve absorption lines,  $\sigma$  likely depends on  $\rho$ ; the  $\rho$  dependence is suggested in a report by Endo *et al.* (2015). However, the results did not demonstrate a clear  $\rho$  dependence, likely because the random errors of  $\sigma$  were much larger than those reported by Endo *et al.* (2015). Pure sulfur isotopologue  $^{32,33,34,36}\text{SO}_2$  cross-sections were calculated from the isotopic purity as reported by the manufacturer (99.99%, 99.80%, 98.80%, and 99.24% for  $^{32}\text{S}$ ,  $^{33}\text{S}$ ,  $^{34}\text{S}$ , and  $^{36}\text{S}$ , respectively).

### Calculating fractionation factors for isotopic self-shielding

Once  $^{32,33,34,36}\text{SO}_2$  cross-sections are determined, the fractionation factors during  $\text{SO}_2$  photolysis can be calculated

as follows (Miller and Yung, 2000):

$${}^{3x}J = \int {}^{3x}\sigma(\lambda) \Phi(\lambda) I_0(\lambda) e^{-\rho L \sigma(\lambda)} d\lambda \quad (4)$$

$${}^{3y}\varepsilon = \ln({}^{3y}J / {}^{32}J) \times 1000 \% \quad (5)$$

$${}^{33}\text{E} = {}^{33}\varepsilon - 0.515 \times {}^{34}\varepsilon \% \quad (6.1)$$

$${}^{36}\text{E} = {}^{36}\varepsilon - 1.90 \times {}^{34}\varepsilon \% \quad (6.2)$$

where  $3x$  represents each sulfur isotope (32, 33, 34, or 36),  $3y$  represents each sulfur isotope excluding  ${}^{32}\text{S}$  (33, 34, or 36),  ${}^{3x}\sigma$  represents the  ${}^{3x}\text{SO}_2$ -absorption cross-section [ $\text{cm}^2$ ],  ${}^{3x}J$  is the  ${}^{3x}\text{SO}_2$ -photolysis rate constant [ $\text{s}^{-1}$ ],  $L$  is the path length [ $\text{cm}$ ],  $\lambda$  is the wavelength [nm], and  $\sigma$  is the natural abundance  $\text{SO}_2$ -absorption cross-section [ $\text{cm}^2$ ] ( ${}^{32}\text{S}/{}^{33}\text{S}/{}^{34}\text{S}/{}^{36}\text{S} = 95.018/0.75/4.215/0.017$ , Farquhar, 2018).  $I_0$  is the incident photon flux [ $\text{cm}^{-2}\text{s}^{-1}\text{nm}^{-1}$ ],  $\Phi$  is the quantum yield of  $\text{SO}_2$  photolysis from Okazaki *et al.* (1997), and  $\rho$  is the  $\text{SO}_2$  number density [ $\text{cm}^{-3}$ ]. Here, the quantum yield is assumed to be the same for all isotopologues since the isotopic effect on the quantum yield is negligible during  $\text{SO}_2$  photolysis (Ono, 2017). Fractionation factors ( ${}^{33}\varepsilon$ ,  ${}^{34}\varepsilon$ ,  ${}^{36}\varepsilon$ ,  ${}^{33}\text{E}$ , and  ${}^{36}\text{E}$ ) were used, where  ${}^{33,34,36}\varepsilon$  represents the magnitudes of fractionation to  ${}^{32}\text{S}$  and  ${}^{33,36}\text{E}$  represents the magnitudes of mass-independent fractionation.

### Assumptions of a simple analytical self-shielding model

Very high spectral resolution and high precision are required to compare fractionation factors predicted by absorption spectra with photolysis experiments. Because such experimental quality is technically difficult to achieve, we modeled self-shielding analytically to capture its trends. Recently, Lyons (2020) reported this phenomenon. In the present paper, we have added this discussion to the present paper.

The difference in absorption wavelength between isotopologues is caused by a difference in vibration frequency. The shifted absorption spectra of  ${}^{32}\text{SO}_2$  were used as the absorption spectra of  ${}^{33,34,36}\text{SO}_2$  (Lyons, 2007). This shift model is valid for approximating reproducible photolysis experiments. Specifically, the shifted spectra were compared with the isotope fractionations observed in  $\text{SO}_2$  photolysis experiments at room temperature (Ono *et al.*, 2013; Endo *et al.*, 2019). The natural abundance  $\text{SO}_2$  absorption spectra reported by Freeman *et al.* (1984) (~0.5  $\text{cm}^{-1}$  of spectral resolution, 213 K; **Table 1**) and Stark *et al.* (1999) (~0.12 or 0.18  $\text{cm}^{-1}$  of spectral resolution, 295 K; **Table 1**) were used as the  ${}^{32}\text{SO}_2$  absorption spectra in Ono *et al.* (2013) and Endo *et al.* (2019), respectively. When the  $\text{SO}_2$  column density increased,  $\delta^{34}\text{S}$  and  $\Delta^{33}\text{S}$  of the products increased in both experiments, and the shift models explained the overall trends. However, this shift did not quantitatively explain the magnitudes of  $\delta^{34}\text{S}$  and  $\Delta^{33}\text{S}$ . In the report by Ono *et*

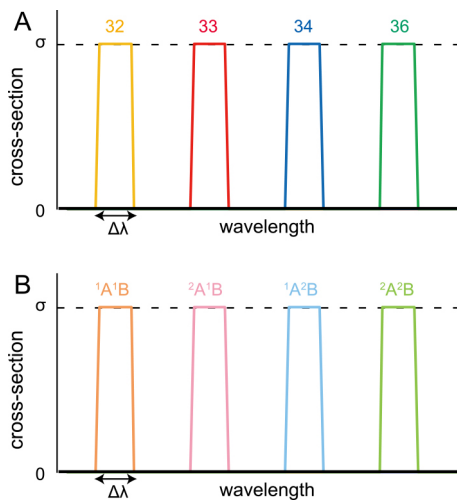


**Fig. 1.** The simplest case of modeled (A)  $^{32,33,34,36}\text{SO}_2$  absorption spectra and (B)  $^1\text{A}'\text{B}$ ,  $^2\text{A}'\text{B}$ ,  $^1\text{A}^2\text{B}$ , and  $^2\text{A}^2\text{B}$ , each of which absorbs different wavelength. The line width is  $\Delta\lambda$ . Cross-sections are  $\sigma$  at wavelength of absorption lines and 0 at wavelength excluding the absorption lines.

al. (2013), the model overestimated the  $\delta^{34}\text{S}$  of the products and predicted a ~1.9 times larger  $\delta^{34}\text{S}/(\text{SO}_2 \text{ column density})$ . They speculated that this discrepancy could be attributable to the difference in temperature. In the study by Endo *et al.* (2019), the model predicted a ~1.15 times larger  $\delta^{34}\text{S}/(\text{SO}_2 \text{ column density})$  and a ~2 times larger  $\Delta^{33}\text{S}/\delta^{34}\text{S}$ . They speculated that this discrepancy was due to errors in the cross-section.

Absorption line widths are nearly the sum of Doppler and pressure widths at the troposphere and stratosphere, because a natural width is much smaller than others. The overlap of absorption spectra may be reduced when photolysis is conducted at low temperature and low total atmospheric pressure or using molecules that have more discrete absorption spectra. The simplest case of self-shielding occurs when the absorption line is narrow (sub-Doppler width) and  $^{32,33,34,36}\text{SO}_2$  absorbs only one wavelength, which depends on isotopologues. In other words, the cross-section is  $\sigma$  at wavelengths of absorption lines and 0 at wavelengths excluding the absorption lines; the absorption line width is  $\Delta\lambda$  (**Fig. 1A**).

Furthermore, as for multiply-substituted isotopologues (called as “clumped isotope”; e.g.,  $^{13}\text{C}^{18}\text{O}^{16}\text{O}$  in case of  $\text{CO}_2$ ; Eiler, 2007), the simplest self-shielding model is useful to capture the nature of the isotope signature. Self-shielding may produce clumped isotope enrichment and depletion, although it has not been found that self-shielded clumped isotope signature is preserved in natural samples in research to date. We modeled the simplest case of molecule AB’s excitation ( $\text{AB} \rightarrow \text{AB}^*$ ). Isotopologues of AB are assumed to be  $^1\text{A}'\text{B}$ ,  $^1\text{A}^2\text{B}$ ,  $^2\text{A}'\text{B}$ , and  $^2\text{A}^2\text{B}$ , with major isotopes of  $^1\text{A}$  and  $^1\text{B}$  and minor isotopes of  $^2\text{A}$  and  $^2\text{B}$ . A unique clumped isotope of the AB

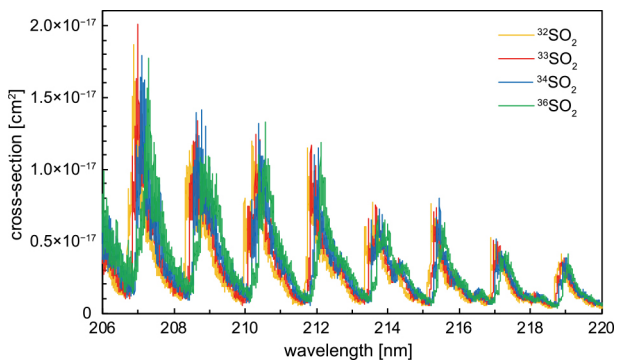


**Fig. 2.** Comparison of measured  $^{32,33,34,36}\text{SO}_2$  absorption cross-sections from 206 to 220 nm. As previously reported (Danielache *et al.*, 2008; Endo *et al.*, 2015; Tokue and Nanbu, 2010), the main absorption band, wherein the bound-bound  $\text{C}^1\text{B}_2\text{-X}^1\text{A}_1$  is the main cause of the observed red-shifting.

molecule was  $^2\text{A}^2\text{B}$ . It was assumed that each isotopologue absorbs a different wavelength (**Fig. 1B**). The analytical calculations and results of the models are described in Section “Calculations of self-shielding using synthesized absorption spectra”.

## Results

### A Absorption spectra measurements

The measured absorption cross-sections are shown in **Figs. 2** and S2. The absorption spectra of  $^{33,34,36}\text{SO}_2$  appeared red-shifted with respect to the  $^{32}\text{SO}_2$  spectrum. Random errors (standard error of 1 s. d.) were approximately 10% following the data treatment as presented in Section “Spectrometry and measurements”. Even at high resolution, such as in this study,  $^{32,33,34,36}\text{SO}_2$  absorption spectra overlap with each other (Fig. S2). The errors in this report are consistent with those of the previous spectra (**Table 1**).

The  $^{32}\text{SO}_2$  absorption spectrum of the present study is compared with four previous measurements of  $^{32}\text{SO}_2$  or natural abundance  $\text{SO}_2$  absorption spectra (Stark *et al.*, 1999; Wu *et al.*, 2000; Danielache *et al.*, 2008; Endo *et al.*, 2015) in **Fig. 3**. The close comparison of the five measurements ranging from low-resolution and high precision (~25 cm<sup>-1</sup>, 1%; Endo *et al.*, 2015) to high resolution and low precision (~0.12 and ~0.18 cm<sup>-1</sup>, 10%–50%; Stark *et al.*, 1999) shows a clear change in the spectrum waveform. A measurement of the high-resolution and precision of isotopically enriched spectra is ideal, yet not realistically achievable. An in-depth analysis of the ideal trade-off between resolution and precision is beyond the scope of this study. Here, we discuss the limits of the required spectral resolution required to account for the waveform features of the spectra. As presented in **Fig. 3**, spectral resolution at 12.5 cm<sup>-1</sup> (Wu *et al.*, 2000) and 25 cm<sup>-1</sup> (Danielache *et al.*, 2008) are comparable, while the resolution at 0.12 cm<sup>-1</sup> (Stark *et al.*, 1999) is significantly lower.

**Table 1.** Summary and comparison of reported  $\text{SO}_2$  absorption spectra. Photolysis rate constants ( $J$  value) are presented for measurements at room temperature. The  $J$  values are those of  $^{32}\text{SO}_2$  for the present study, Danielache *et al.* (2008), and Endo *et al.* (2015) or natural abundance  $\text{SO}_2$  for Stark *et al.* (1999) and Wu *et al.* (2000). They were calculated from Eq. (4), where  $I_0(\lambda)$  is 1,  $L$  is 0, and  $\Phi$  is from Okazaki *et al.* (1997).

Reference	Isotope	Spectral range (nm)	Resolution ( $\text{cm}^{-1}$ )	Precision (%)	$J$ (206–220 nm, $10^{-17} \text{ s}^{-1}$ )	Temp (K)
The present study	$^{32}\text{S}, ^{33}\text{S}, ^{34}\text{S}, ^{36}\text{S}$	206–220	1	~10	4.18	295
Stark <i>et al.</i> (1999)	natural abundance	198–220	0.18, 0.12	~10–50	4.29	295
Wu <i>et al.</i> (2000)	natural abundance	175–295	12.5	<10	4.22	200–400
Danielache <i>et al.</i> (2008)	$^{32}\text{S}, ^{33}\text{S}, ^{34}\text{S}$	183–350	25	~1.2	4.95	293
Endo <i>et al.</i> (2015)	$^{32}\text{S}, ^{33}\text{S}, ^{34}\text{S}, ^{36}\text{S}$	190–225	25	~1	5.28	293
Freeman <i>et al.</i> (1984)	natural abundance	170–240	0.5	~4		213
Vandaele <i>et al.</i> (1994)	natural abundance	250–333	2	~2.5		296
Koplow <i>et al.</i> (1998)	natural abundance	215.21–215.23	0.0003	N/A		295
Rufus <i>et al.</i> (2003)	natural abundance	220–325	0.12	~5		295
Rufus <i>et al.</i> (2009)	natural abundance	199–220	0.18, 0.12	~12–50		160
Hermans <i>et al.</i> (2009)	natural abundance	227–345	2	~1.5		298–358
Vandaele <i>et al.</i> (2009)	natural abundance	345–416	2	~4–6		298–358
Blackie <i>et al.</i> (2011)	natural abundance	212–325	0.12	~4.5		198
Danielache <i>et al.</i> (2012)	$^{32}\text{S}, ^{33}\text{S}, ^{34}\text{S}, ^{36}\text{S}$	250–320	8	~2.5		293

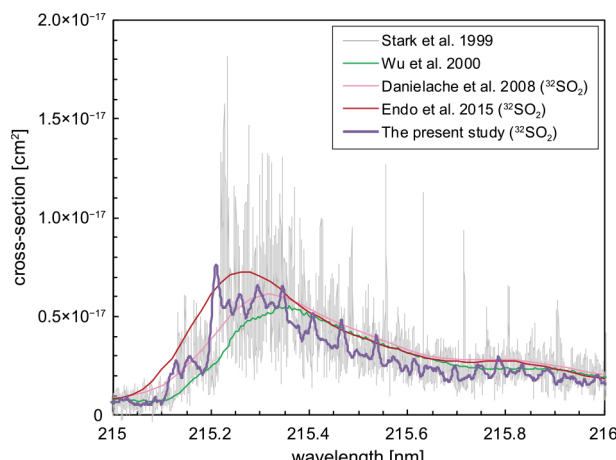


**Fig. 3.** Comparison of five measurements including the present study at different spectral resolution (See Table 1 for spectral details). All of the displayed spectra were measured at room temperature. The differences in the waveform can be attributed to the spectral resolution of the measurement.

*al.*, 2008; Endo *et al.*, 2015) were not capable of capturing the fine features of a high-resolution spectrum as reported by Stark *et al.* 1999 ( $\sim 0.12$  and  $\sim 0.18 \text{ cm}^{-1}$ ). The spectral resolution of  $1 \text{ cm}^{-1}$  in this report shows sharp features; however, the fine structure, most likely produced by either a single or a combination of multiple ro-vibrational electronic transitions, is not fully resolved. A key question to address is whether these spikes in the spectra, regardless of how visually large they appear, significantly contribute to the photolysis rate constant, and its associated isotopic effect.

To aid understanding of the trade-off between spectral

resolution and precision, a comparison between these measurements and the data reported by Stark *et al.* (1999) is presented in Fig. S3. Narrow-band, tunable, frequency-quadrupled diode laser measurements carried out by Koplow *et al.* (1998) estimated that a spectral resolution of below  $\sim 0.1 \text{ cm}^{-1}$  is required to resolve the highly structured spectra of the  $\text{SO}_2$  molecule. The data reported by Stark *et al.* (1999) is the closest to the required spectral resolution to achieve a fully resolved spectrum ( $\sim 0.12$  and  $\sim 0.18 \text{ cm}^{-1}$ ). When these spectra are used to calculate the photolysis rate constants for rare isotopologues, there is a need for high precision. Stark *et al.* (1999) reported minimum and maximum cross-section errors ranging from 10% to 50%. We converted these values to actual cross-sections and compared them against the data presented in this report. The spectral range presented in Fig. S3 was selected from the study by Koplow *et al.* (1998). This spectral region shows an absorption peak with a maximum SN ratio, which is a 10% error for Stark *et al.* (1999). In comparison, the data in this report for the same spectral range contain an error rate between 3% and 4%. Although inferences from synthetic isotopologue spectra derived from this spectrum may be appealing due to their high spectral resolution and importance to self-shielding phenomena, errors that will be propagated to fractionation factors must be considered when applying such spectra to geochemical processes.

The spectral resolution in this report was 25 times higher than that of the previously reported  $\text{SO}_2$  isotopologues spectra. To confirm the wavelength accuracy, natural  $\text{SO}_2$  absorption spectra of our results were compared with the spectra reported by Stark *et al.* (1999) and the

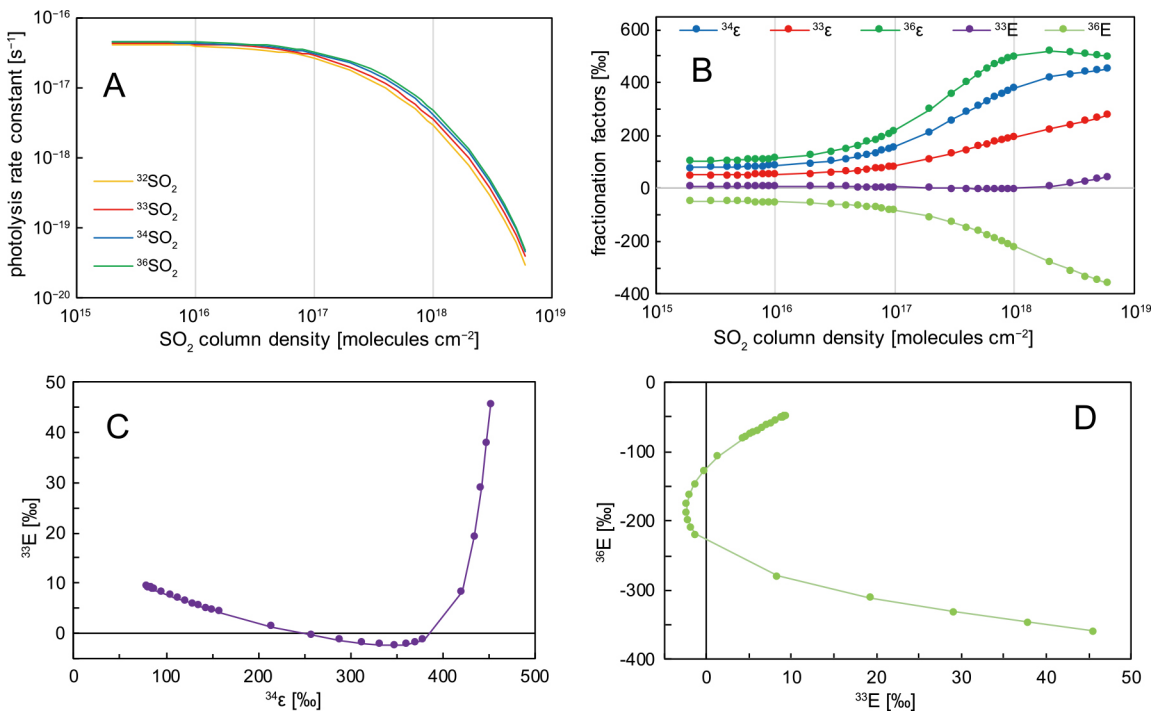


**Fig. 4.** Using measured absorption spectra, estimation of (A) <sup>32,33,34,36</sup>SO<sub>2</sub> photolysis rate constants (<sup>3x</sup>J values) vs. SO<sub>2</sub> column density, (B) <sup>33,34,36</sup>ε and <sup>33,36</sup>E values vs. SO<sub>2</sub> column density, and (C) a three-isotope plot of <sup>34</sup>ε and <sup>33</sup>E, and (D) four-isotope plot of <sup>33</sup>E and <sup>36</sup>E. Error bars are smaller than symbols.

spectra convolved with a 1-cm<sup>-1</sup> (FWHM) Gaussian function (Fig. S4). We noticed that a wavelength shift of ~0.016 nm exists between the convoluted and the spectra presented in this report (Fig. S4). The wavelength calibration of the VERTEX80v is based on the wavelength of the He–Ne laser fixed at 15.798 cm<sup>-1</sup>, and is therefore, in principle, exact. The cause of the observed ~0.016 nm difference is not clear. Further calibration of wavelengths in the UV region can be performed by using the absorption band of a well-known molecule such as O<sub>2</sub> or NO<sub>2</sub>. We opted to use the literature spectra to calibrate the wavelength of our measurements. The wavelength scale by Stark *et al.* (1999) reproduces that reported by Freeman *et al.* (1984) and Koplow *et al.* (1998), although spectrometers and wavelength calibration methods vary among the three reports. The calibration procedure consisted of shifting the spectrum by 17 wavenumber steps or 4.0984 cm<sup>-1</sup> (~0.0164 nm). Following wavelength calibration, the <sup>32</sup>SO<sub>2</sub> spectrum replicated the literature data reasonably well (Figs. S4 and S5).

Next, the magnitudes of the cross-sections were evaluated against data in the literature (Fig. S5). The magnitudes of the measured cross-sections at some wavelengths were smaller than that of the literature data. Of note, these discrepancies are larger at absorption peaks due to insufficient spectral resolution. For highly structured spectra such as SO<sub>2</sub>, measurements under insufficient spectral resolution may yield significantly smaller cross-sections than those measured at high resolution.

### Isotopic self-shielding estimation using measured cross-sections

We calculated the fractionation factors using our spectroscopic measurements (Eqs. 4–6) (Figs. 4 and 5). Fig. 4 shows the values of SO<sub>2</sub> photolysis rate constants (<sup>32</sup>J) (A) and fractionation factors (B) vs. SO<sub>2</sub> column density (from 2 × 10<sup>15</sup> to 7 × 10<sup>18</sup> cm<sup>-2</sup>), and a three- or four-isotope plot (C and D) in which the incident photon flux is constant against wavelength ( $I_0(\lambda) = 1$ ). The C band absorption, where SO<sub>2</sub> is photolyzed, is located from 165 to 219.2 nm. In assumed Archean atmospheres, carbon dioxide (CO<sub>2</sub>) scatters most of the <190-nm UV photons. The SO<sub>2</sub> photolysis rate constant (the J value in Eq. 4) between 206 and 220 nm is approximately 2/3rd of that between 190 and 220 nm (Endo *et al.*, 2015). The calculation assumes that the fractionations, including self-shielding, do not vary based on the wavelength. Therefore, the calculation may be more accurate when absorption spectra below 206 nm are reported.

Random errors of <sup>33,34,36</sup>ε value ( $\Delta^{33,34,36}\epsilon$ ) are calculated as functions of <sup>32,33,34,36</sup>σ<sub>i</sub>:

$$|\Delta^{3y}\epsilon| = \left| \sum_{i=1}^n \left[ \frac{\partial^{3y}\epsilon}{\partial^{32}\sigma_i} \Delta^{32}\sigma_i + \frac{\partial^{3y}\epsilon}{\partial^{3x}\sigma_i} \Delta^{3x}\sigma_i \right] \right| \quad (7)$$

$$\frac{\partial^{3x}\epsilon}{\partial^{32}\sigma_i} = - \frac{\int I d\lambda}{\int^{32}\sigma_i I d\lambda} \quad (8)$$

$$\frac{\partial^{3y}\epsilon}{\partial^{3y}\sigma_i} = - \frac{\int I d\lambda}{\int^{3y}\sigma_i I d\lambda} \quad (9)$$

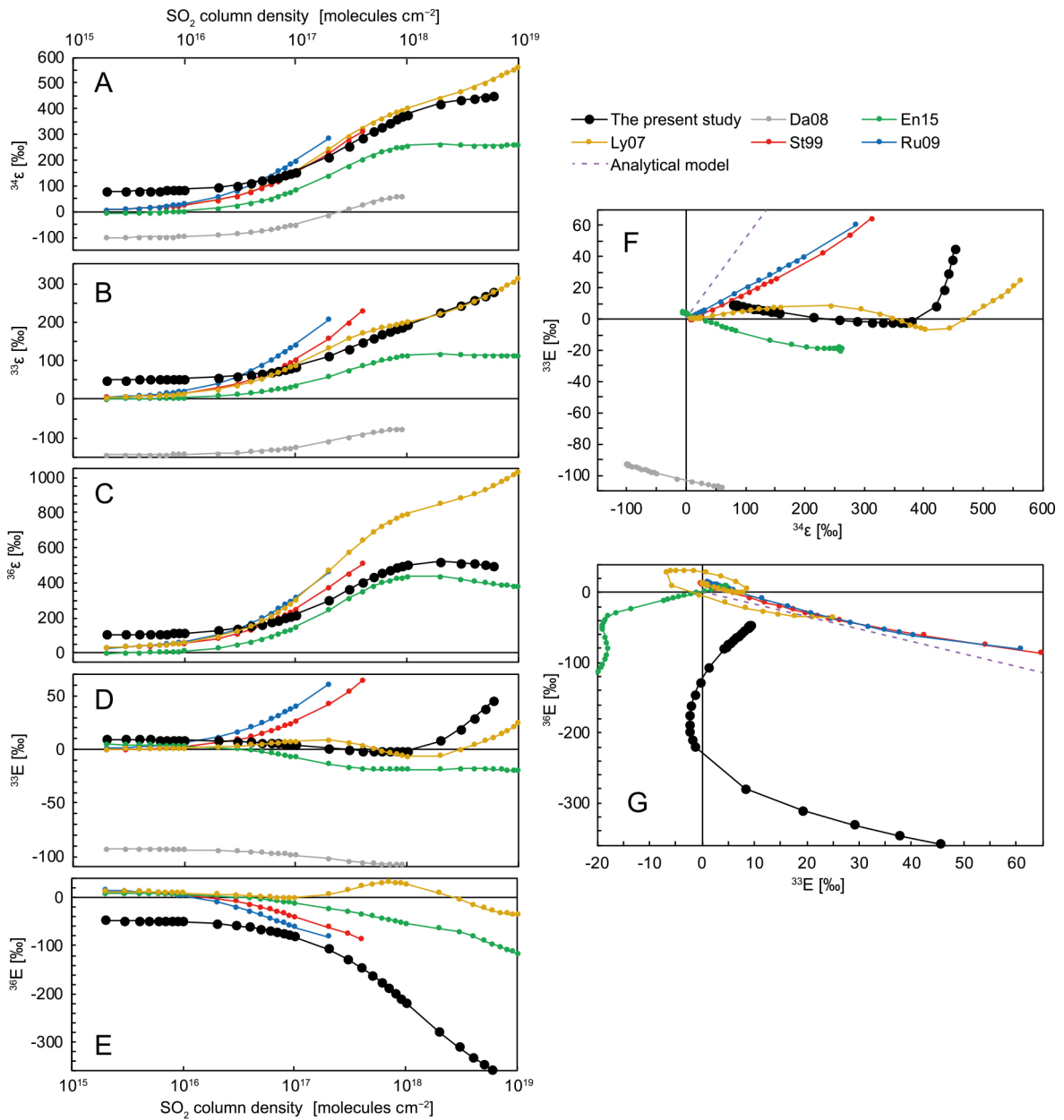


**Fig. 5.** Calculated fractionation factors by  $\text{SO}_2$  isotopologues absorption cross-sections. Plots of ((A)  ${}^{34}\epsilon$ , (B)  ${}^{33}\epsilon$ , (C)  ${}^{36}\epsilon$ , (D)  ${}^{33}E$ , and (E)  ${}^{36}E$ ) vs.  $\text{SO}_2$  column density, (F)  ${}^{34}\epsilon$  vs.  ${}^{33}E$ , and (G)  ${}^{33}E$  vs.  ${}^{36}E$ . Black, gray, green, gold, red, and blue lines represent the present study, Danielache *et al.* (2008), Endo *et al.* (2015), Lyons (2007), Stark *et al.* (1999), and Rufus *et al.* (2009), respectively. Cross-sections of  ${}^{33,34,36}\text{SO}_2$  of Stark *et al.* (1999) and Rufus *et al.* (2009) are the red shift model. We used the shifting parameters from Figure 8 of Tokue and Nanbu (2010). Cross-sections of  ${}^{33,34,36}\text{SO}_2$  of Lyons (2007) are also the red shift model (see text). Wavelength ranges of all plots are from 206 to 220 nm in Eq. (4). Assumed photon spectra are flat (does not depend on wavelength). Calculated  $\text{SO}_2$  column density is from  $2 \times 10^{15}$  to  $10^{19} \text{ cm}^{-2}$ , and the column density range is limited in case that  ${}^{32}J$  is larger than 2 s.d. of  ${}^{32}J$ . Purple dashed lines in (F) and (G) represent the analytical model in the case of narrow absorption lines.

where  $n$  is the number of wavelength grids,  $\sigma_i$  is the cross-section of the  $i$ -th wavelength step, and  $I (= I_0 e^{-\rho {}^{32}J})$  is the photon spectra after shielding; shielding by  ${}^{32}\text{SO}_2$  spectra is assumed in this calculation. Because the number of divided wavelength steps is quite large ( $n = 12,791$ ), typical random errors of  ${}^{33,34,36}\epsilon$  and  ${}^{33,36}E$  values from Eqs. (7)–(9) are approximately 5‰ at an  $\text{SO}_2$  column density ( $\rho L$ ) of  $10^{19} \text{ cm}^{-2}$  or less. The random errors are not shown in **Figs. 4** and **5** because they are signifi-

cantly smaller than the graphs' range. Signal drift errors (up to 4.5%, estimated in Section “Spectrometry and measurements”) were not included in the above random errors. In this calculation, drift errors are added to  ${}^{33,34,36}\epsilon$  and  ${}^{33,36}E$  at all  $\text{SO}_2$  column densities; therefore, they are not assumed to significantly contribute to  ${}^{33,34,36}\epsilon/(\text{SO}_2 \text{ column density})$ ,  ${}^{33,36}E/(\text{SO}_2 \text{ column density})$ ,  ${}^{33}E/{}^{34}\epsilon$ , and  ${}^{36}E/{}^{33}E$  calculations.

**Fig. 4A** presents a wide range of  ${}^{32}J$  values, some of

which are within plausible photolysis conditions for an Archean atmosphere. The  ${}^{32}J$  values for column densities above  $10^{18}$  cm $^{-2}$  are, in terms of kinetics, insignificant. From  $10^{17}$  to  $10^{18}$  cm $^{-2}$  of SO<sub>2</sub> column density, where  ${}^{32}\text{SO}_2$  is optically thick, all  ${}^{33,34,36}\epsilon$  values increase and significant self-shielding occurs (Fig. 4B). The capital epsilon values ( ${}^{33,36}\text{E}$ ) are more complex and more sensitive to SO<sub>2</sub> column density than the  ${}^{33,34,36}\epsilon$  values (Fig. 4B). As presented in Fig. 4B and C,  ${}^{34}\epsilon$  increased, but  ${}^{33}\text{E}$  decreased. This trend is different from the observed MIF-S in most previous SO<sub>2</sub> photolysis experiments (see Section ‘‘Comparison to photochemical experiments’’). At  $\sim 10^{18}$  cm $^{-2}$  of SO<sub>2</sub> column density, the  ${}^{34}\epsilon$ ,  ${}^{36}\epsilon$ , and  ${}^{33}\text{E}$  trends changed. In particular,  ${}^{33}\text{E}$  started increasing. This is likely due to shielding by not only  ${}^{32}\text{SO}_2$  but also  ${}^{34}\text{SO}_2$ , as estimated by Lyons (2020).

As explained in Section ‘‘Absorption spectra measurements’’, the spectral resolution in this study was lower in comparison to previously reported data (Stark *et al.*, 1999). The lack of spectral resolution resulted in cross-sections of reduced magnitude. Additionally, the wavelength of the reported spectra was adjusted to a convolved spectrum reported by Stark *et al.* (1999). The lack of spectral resolution and potential errors introduced during the wavelength adjustment procedure can introduce errors in the calculation of fractionation factors. To quantify the magnitude of these errors, fractionation factors were calculated using the assumption that only the  ${}^{32}\text{SO}_2$  absorption spectrum was shifted (Fig. S6). The  ${}^{32}\text{SO}_2$  absorption spectrum was shifted by 17 wavenumber steps, 4.0984 cm $^{-1}$  ( $\sim 0.0164$  nm), and fractionation factors were calculated (Fig. S6, light green lines). The  ${}^{32}\text{SO}_2$  absorption spectrum was assumed to be the convolved spectra with 1 cm $^{-1}$  per Stark *et al.* (1999). Since all isotopologues were analyzed in similar ways, the displayed discrepancy represents an upper limit. The uncertainty did not change the overall trend; that is,  ${}^{33,34,36}\epsilon$  increased, but  ${}^{36}\text{E}$  decreased and  ${}^{33}\text{E}$  reversed from decreasing to increasing when the SO<sub>2</sub> column density increased. The uncertainties of the fractionation factors of  ${}^{33,34,36}\epsilon$  were within approximately 30‰ (Fig. S6A–C); thus, they did not contribute to significant errors in the fractionation factors. The uncertainties of the fractionation factors of  ${}^{33,36}\text{E}$  were within approximately 25‰ (Fig. S6D and E). The uncertainties of  ${}^{33}\text{E}/{}^{34}\epsilon$  and  ${}^{36}\text{E}/{}^{33}\text{E}$  were sometimes large (Fig. S6F and G).

The calculated fractionation factors were compared with those reported in previous studies (Fig. 5). Low-resolution absorption spectra of  ${}^{33,34,36}\text{SO}_2$  are available ( $\sim 25$  cm $^{-1}$ , Danielache *et al.*, 2008; Endo *et al.*, 2015). However, because high-resolution  ${}^{33,34,36}\text{SO}_2$  absorption spectra have not been reported, the red-shift model (Danielache *et al.*, 2008) was used for the natural abundance SO<sub>2</sub> absorption spectra per Stark *et al.* (1999) and Rufus *et al.* (2009) (details in Table 1, Rufus *et al.* meas-

ured at 160 K) to produce synthetic  ${}^{33,34,36}\text{SO}_2$  spectra. Natural abundance ( ${}^{32}\text{S}$  of 95%) SO<sub>2</sub> absorption spectra were assumed to be  ${}^{32}\text{SO}_2$  absorption spectra, and the shifted parameters were extracted from Tokue and Nanbu (2010). Additionally, we displayed fractionation factors calculated from the  ${}^{32,33,34,36}\text{SO}_2$  cross-sections by Lyons (2007), as shown in Fig. 5.  ${}^{33,34,36}\text{SO}_2$  absorption spectra from his study were also obtained from red-shifted natural abundance SO<sub>2</sub> absorption spectra; the natural abundance SO<sub>2</sub> absorption spectra were obtained from Freeman *et al.* (1984) (a resolution of  $\sim 0.5$  cm $^{-1}$  and a temperature of 213 K) and the shifting parameters were extracted from Ran *et al.* (2007).

### Calculations of self-shielding using synthesized absorption spectra

Isotope fractionation by self-shielding occurs under conditions in which the absorption line is narrow and  ${}^{32,33,34,36}\text{SO}_2$  absorbed only one wavelength, which varies on isotopologues as described in Section ‘‘Assumptions of a simple analytical self-shielding model’’ (Fig. 1A). An optical depth ( $\tau$ ) is defined here as the natural abundance SO<sub>2</sub> column density ( $\rho'$ ) multiplied by the magnitude of the peak cross-section of each isotopologue ( $\sigma$ , Fig. 1) as  $\rho'\sigma$ . The  ${}^{3x}J$  values are  $\sigma\Delta\lambda \exp(-\tau {}^{3x}N)$ , from Eq. (4), where  ${}^{3x}N$  is the abundance of  ${}^{3x}\text{S}$  of SO<sub>2</sub>. From Eqs. (5), (6),  ${}^{3y}\epsilon$  is  $1000\tau({}^{32}N - {}^{3y}N)\sigma$  ‰,  ${}^{33}\text{E}$  is  $1000\tau(0.485 \times {}^{32}N - {}^{33}N + 0.515 \times {}^{34}N)$  ‰, and  ${}^{36}\text{E}$  is  $1000\tau(-0.90 \times {}^{32}N - {}^{36}N + 1.90 \times {}^{34}N)$  ‰. The slopes of  ${}^{33}\text{E}/{}^{34}\epsilon$  and  ${}^{36}\text{E}/{}^{33}\text{E}$  are functions of isotope abundance only. (These equations are the same as those in Eq. 20 in Lyons, 2020).

When the typical sulfur isotope abundance on Earth ( ${}^{32}\text{S}/{}^{33}\text{S}/{}^{34}\text{S}/{}^{36}\text{S} = 95.018/0.75/4.215/0.017$ , Farquhar, 2018) is assumed, the slopes of  ${}^{33}\text{E}/{}^{34}\epsilon$  and  ${}^{36}\text{E}/{}^{33}\text{E}$  are +0.523 and -1.63; these slopes are shown in Fig. 5F and G for comparison.  ${}^{34}\epsilon$  and  ${}^{33}\text{E}$  are +908τ ‰, and +475τ ‰, respectively. The modeled  ${}^{33}\text{E}/{}^{34}\epsilon$  (+0.52) slope is closer to the Archean slope ( $\sim +0.9$ ; Ono *et al.*, 2009) in comparison to the trends observed in SO<sub>2</sub> photolysis ( $\sim 0.1$ ; Ono, 2017). In addition, the optical depth for self-shielding was assumed to be  $\geq 1$  (Lyons, 2007; Claire *et al.*, 2014), but significant self-shielding may occur even when the optical depth is  $\sim 0.1$ .

Additionally, we tested the sensitivity of isotope abundance. In the case of +100‰ fractionation of  $\delta^{34}\text{S}$  mass-dependently ( ${}^{32}\text{S}/{}^{33}\text{S}/{}^{34}\text{S}/{}^{36}\text{S} = 94.558/0.789/4.636/0.017$ ),  ${}^{33}\text{E}/{}^{34}\epsilon$  and  ${}^{36}\text{E}/{}^{33}\text{E}$  were +0.528 and -1.60, respectively. Sulfur isotope abundance had insignificant effects on  ${}^{33}\text{E}/{}^{34}\epsilon$  and  ${}^{36}\text{E}/{}^{33}\text{E}$ .

The linear-scale fractionation factors are suitable for considering mixing; the values of  ${}^{33,34,36}\epsilon$  used can be found by the following equation:

$${}^{3y}\epsilon = 1000 \times ({}^{3y}J / {}^{32}J - 1) \text{ ‰} \quad (5')$$

where  $^{33,36}\epsilon$  values are the same as those in Eqs. 6.1 and 6.2. In the narrow absorption line scenario,  $^{3y}\epsilon$  is  $1000[\exp(\tau^2N - \tau^3N) - 1]\%$ . The slopes of  $^{33}E/^{34}E$  and  $^{36}E/^{33}E$  depend on the optical depth and are sometimes similar to those of the Archean slope. For example, at  $\tau = 5$ ,  $^{33}E/^{34}E$  and  $^{36}E/^{33}E$  were 0.668 and -1.01, respectively.

Next, we calculated the clumped isotope enrichment or depletion in self-shielding in the excitation of AB molecules ( $AB \rightarrow AB^*$ ). It was assumed that the four isotopologues absorb different wavelengths (Section “Assumptions of a simple analytical self-shielding model” and Fig. 1B). The fractionation factor of clumped isotope enrichment in kinetic reactions,  $^{2A,2B}\gamma$ , was defined as (see Section 3.2 of Whitehill *et al.*, 2017):

$$^{2A,2B}\gamma = \left( ^{2A,2B}J \times ^{1A,1B}J \right) / \left( ^{2A}J \times ^{2B}J \right) \quad (10)$$

where  $^{2A}J$ ,  $^{2B}J$ , and  $^{xA,xB}J$  represent the excitation rate constants of  $^2AB$  (weighted average considering abundance of  $^2A^1B$  and  $^2A^2B$ ),  $A^2B$  (weighted average considering abundance of  $^1A^2B$  and  $^2A^2B$ ), and  $^{xA}xB$  isotopologues, respectively (Wang *et al.*, 2016). To capture the natural abundance, assuming that the isotopologues except  $^1A^1B$  are rare, the  $^{2A,2B}\gamma$  is approximately equal to  $e^{-\tau}$ , where  $\tau$  is a product of the cross-section at the peak wavelength, ( $\sigma$ , Fig. 1B), and column density of the AB molecule ( $\rho'$ ). The deformations are described in the Supporting Information (Supporting text 1). The log scale of  $^{2A,2B}\gamma$  is

$$\ln(^{2A,2B}\gamma) \approx -\tau \quad (11)$$

By multiplying both sides of Eq. (11) by 1000, we obtained the clumped isotope enrichment factor in permil (‰). Consequently, the clumped isotope depletion (‰) in the product ( $AB^*$ ) was approximately 1000 times larger than the optical depth. Next, in a closed system, the clumped isotope compositions ( $\Delta$ , the deviation from a stochastic distribution) for the reagent (AB) obey Rayleigh fractionation (in Section A.2 of Whitehill *et al.*, 2017). Under the assumption that isotopologues are rare with the exception of  $^1A^1B$ , the difference in the clumped isotope composition in the reagent is:

$$\Delta - \Delta_0 \approx 1000(1 - e^{-\tau}) \times \ln f \quad \text{‰} \quad (12)$$

where  $f$  is the remaining fraction,  $\Delta$  is the clumped isotope composition at the remaining fraction of  $f$ , and  $\Delta_0$  is the initial clumped isotope composition. The deformations are described in Supporting Information (Supporting text 1). Because  $\ln f$  is negative,  $\Delta - \Delta_0$  is positive. Thus, self-shielding led to clumped isotope enrichment in the reagent. In addition, the clumped isotope is a deviation in a single molecule rather than a fractionation; therefore, mass balance is not strictly conserved (net capital delta is not necessarily 0). In accordance with this, large enrichment or depletions will be recorded in major

chemical species (for example, in atmospheric N<sub>2</sub>; Yeung *et al.*, 2017).

## Discussion

We focused on self-shielding, that is, the SO<sub>2</sub> column density dependence. In Section “Comparing with previous SO<sub>2</sub> absorption spectra”, we qualitatively discuss self-shielding trends using the present and previous SO<sub>2</sub> spectral studies. In Section “Comparison to photochemical experiments”, the trends are discussed using both spectral studies and isotope fractionations in previous photolysis experiments, and we attempt to explain them quantitatively. Despite many efforts, the Archean MIF-S trends have not been sufficiently reproduced. In Section “Applying a self-shielding model using the synthesized absorption spectra to laboratory experiments and natural samples”, we discuss the application of the analytical self-shielding model.

### Comparing with previous SO<sub>2</sub> absorption spectra

Owing to the fine structure of the SO<sub>2</sub> absorption spectra, it is believed that high wavelength resolution spectra are required to predict the self-shielding effect. The highest resolution measurements of SO<sub>2</sub> from 206 to 220 nm have been reported by Stark *et al.* (1999) at 295 K and by Rufus *et al.* (2009) at 160 K. Their resolutions were  $\sim 0.12 \text{ cm}^{-1}$ , which does not completely resolve the Doppler width ( $\sim 0.072 \text{ cm}^{-1}$ ). The resolutions of this study, Danielache *et al.* (2008), and Endo *et al.* (2015) were  $\sim 1$ ,  $\sim 25$ , and  $\sim 25 \text{ cm}^{-1}$ , respectively, which did not resolve either of the isolated rotational lines.

As illustrated in Fig. 5, the predicted fractionation factors showed a correlation with the spectral resolution between Stark *et al.* (1999) and the present study at a constant temperature, where the  $^{33,34,36}\epsilon$  values increased with the resolution. The absorption peak magnitudes are larger and the optical depth is apparently larger at higher resolutions, so that the effects of resolution could be qualitatively predicted. Meanwhile, the lower temperature absorption spectra at the same resolution was predictive of larger  $^{33,34,36}\epsilon$  values. The effects of temperature can also be qualitatively predicted because the magnitudes of the absorption peaks are larger at lower temperatures (Rufus *et al.*, 2009; Wu *et al.*, 2000). Since both the resolution ( $\sim 0.5 \text{ cm}^{-1}$ ) and the temperature (213 K) used by Lyons (2007) were different from those used in other reports, the results cannot be compared directly with other reports. However, both the resolution and temperature were between those of this study and the one by Rufus *et al.* (2009). At SO<sub>2</sub> column densities less than  $2 \times 10^{17} \text{ cm}^{-2}$ , the  $^{33,34,36}\epsilon$  values predicted by Lyons (2007) were between those obtained in this study and by Rufus *et al.* (2009) (Fig. 5A–C); this retains consistency with the relationships previously described.

The capital E values ( $^{33,36}\text{E}$ ) are complex because they possess relationships with two  $^{3x}\epsilon$  values. Notably,  $^{33}\text{E}$  (or  $^{33}\text{E}/^{34}\epsilon$ ) was sensitive to the resolution (Fig. 5F). Previous photolysis experiments have demonstrated that the isotope fractionation during  $\text{SO}_2$  photolysis is sensitive to total pressure and, likely, the absorption line width. Additionally,  $^{33}\text{E}$  was found to decrease at broad absorption lines (Endo *et al.*, 2019; Masterson *et al.*, 2011). This is consistent with the small or negative  $^{33}\text{E}$  in the case of the low-resolution spectra discussed in Section “Comparison to photochemical experiments”.

### Comparison to photochemical experiments

The isotope fractionation factors of  $\text{SO}_2$  photolysis estimated by the absorption spectra in this study were compared with previous  $\text{SO}_2$  photolysis experiments. Figure 6 represents the  $\text{SO}_2$  column density dependence, and Fig. 7 represents the total pressure dependence, which was assumed to be the absorption line width dependence. The data of the photolysis experiments shown in Fig. 6 were obtained following calibrations and filtering. In laboratory experiments, the  $\text{SO}_2$  column density depends on the distance from the window of the UV source side, thus the  $J$  value in Eq. (4) is integrated with respect to distance  $L$  (Eq. 4 in Endo *et al.*, 2019).

$$^{3x}J = \iint {}^{3x}\sigma(\lambda) \Phi(\lambda) I_0(\lambda) e^{-\rho L \sigma(\lambda)} d\lambda dL \quad (13)$$

The fractionation factors ( $^{33,34,36}\epsilon$  and  $^{33,36}\text{E}$ ) were calculated using the same equations, that is, Eqs. (5) and (6), respectively: The isotope compositions ( $\delta^{33,34,36}\text{S}$  and  $\Delta^{33,36}\text{S}$ ) of products in photolysis experiments are sometimes significantly different from fractionation factors ( $^{33,34,36}\epsilon$  and  $^{33,36}\text{E}$ ) owing to Rayleigh fractionation. Specifically, fractionation factors are compared with the isotope compositions of products in flow experiments; however, they are not compared with the compositions in static experiments. In static experiments, fractionation factors were estimated by Rayleigh fractionation model or were assumed to be equal to the isotope compositions in the case of small product yields (below 2%). Moreover, the photolysis experiment data were selected and filtered: self-shielding was identified as the dominant isotope fractionation and the  $\text{SO}_2$  column densities were clearly reported; isotopic effects produced by photoexcitation or single-band photolysis were not included in the comparison.

The self-shielding trend is dependent on the total pressure, which is likely attributable to the pressure broadening of  $\text{SO}_2$  absorption lines (Endo *et al.*, 2019). This trend may also depend on temperature; however, this relationship remains unclear (Whitehill *et al.*, 2015; Ignatiev *et al.*, 2019). The room-temperature experiments are shown in Fig. 6. Experiments are divided into two groups: lower total pressure (Fig. 6, open circles; less than 0.1 bar under  $\text{N}_2$  or  $\text{CO}$  atmosphere or less than

0.033 bar pure  $\text{SO}_2$  atmosphere) and higher total pressure (Fig. 6, filled squares; more than 0.1 bar under  $\text{N}_2$  or  $\text{CO}$  atmosphere or more than 0.033 bar pure  $\text{SO}_2$  atmosphere). Fractionation factors hardly depend on total pressure when the total pressure is below 0.1 bar under  $\text{N}_2$  or  $\text{CO}$  atmosphere. However, they demonstrate a dependent relationship with the total pressure when the total pressure is above 0.1 bar under  $\text{N}_2$  or  $\text{CO}$  atmospheres (Endo *et al.*, 2019). The threshold of a pure  $\text{SO}_2$  atmosphere is unknown. The pressure broadening of individual absorption lines can explain the isotopic effect observed in the chamber experiments as summarized above. There are no reported data on the self-pressure broadening effects of  $\text{SO}_2$  in the ultraviolet region. Using the relationship between  $\text{N}_2$  and  $\text{SO}_2$  of the pressure broadening coefficients in the IR region, the self-pressure broadening coefficient of  $\text{SO}_2$  would be approximately three times as large as that of the  $\text{N}_2$  bath gas case. A 0.033-bar (1/3 of  $\text{N}_2$ ) threshold was determined. Pressure broadening coefficients and the HITRAN2016 database were used (Tasinato *et al.*, 2010, 2013, 2014; Gordon *et al.*, 2017; Sumpf *et al.*, 1996a, 1996b; Sumpf, 1997; Ball *et al.*, 1996; Kühnemann *et al.*, 1992; Cazzoli and Puzzarini, 2012). See the Supporting Information (Supporting text 2) for further details. Lower total pressure data (Fig. 6; open circles) seems to follow the column density line, whereas higher total pressure data (Fig. 6; filled squares) seems to be scattered.

Self-shielding appears to begin at  $\sim 10^{16}$  and become fully saturated at  $\sim 5 \times 10^{18} \text{ cm}^{-2}$  of the  $\text{SO}_2$  column density (Fig. 6). To compare  $\text{SO}_2$  photolysis experiments easily, fractionation factors are offset (dashed lines in Fig. 6):  $^{33}\epsilon$ ,  $^{34}\epsilon$ , and  $^{36}\epsilon$  are subtracted by 26‰, 49‰, and 47‰, respectively, such that  $^{33}\text{E}$  is subtracted by 1‰ and  $^{36}\text{E}$  is added by 46‰ (from Eqs. 6.1, 6.2). The magnitude of the offsets is within the range of uncertainty: systematic errors of spectroscopy (up to 4.5%, i.e., 45‰, caused by the drift of the light source), a difference in the UV source spectra, and/or fractionations in the chamber about  $\delta^{34}\text{S}$  (typically 10‰ of  $^{34}\epsilon$  and 0‰ of  $^{33,36}\text{E}$  from the reaction of  $\text{SO}_2 + \text{OH}$ ; Harris *et al.*, 2012).

With respect to  $^{34}\epsilon$  (Fig. 6A and B), at  $< 10^{18} \text{ cm}^{-2}$  of  $\text{SO}_2$  column density, the  $^{34}\epsilon/\text{SO}_2$  column density in this study reproduced laboratory photolysis experiments within approximately 20‰ variation of  $^{34}\epsilon$ , which was only weakly dependent on the total pressure. Inversely, the predicted negative  $^{33}\text{E}/\text{column density}$ , which was dependent on the total pressure, did not match the results of previous experiments (Fig. 6G and H).

To date, no photolysis experiments have reported fractionation factors under experimental conditions ( $< 10^{18} \text{ cm}^{-2}$  of column density and  $\sim 1 \text{ cm}^{-1}$  of line width) such that the results may be compared with this study. Thus, the total pressure and column density dependence systematically tested by Endo *et al.* (2019) were extrapolated.

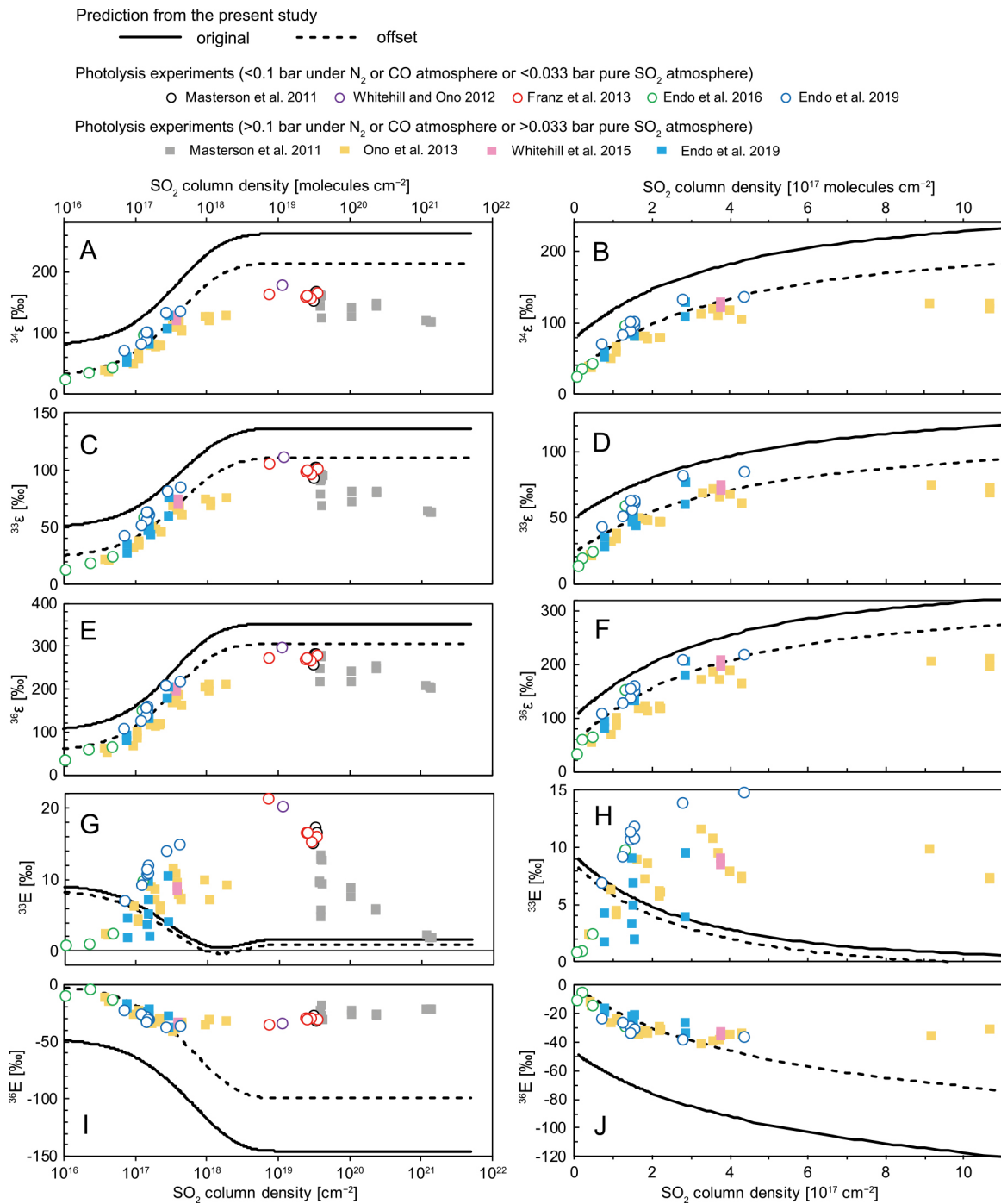


**Fig. 6.** Comparison between fractionation factors predicted by this study (black lines; and dashed lines are offset for comparison) and MIF-S of previous  $\text{SO}_2$  photolysis experiments ((A, B)  $^{34}\epsilon$ , (C, D)  $^{33}\epsilon$ , (E, F)  $^{36}\epsilon$ , (G, H)  $^{33}\text{E}$  and, and (I, J)  $^{36}\text{E}$ ), as functions of  $\text{SO}_2$  column density. Panels A, C, E, G, and I present log scales of wide range of  $\text{SO}_2$  column density, and panels B, D, F, H, and J present linear scales of narrow range. Data are from pure  $\text{SO}_2$  of Masterson *et al.* (2011), DFS-3 of Whitehill and Ono (2012), front cell of Ono *et al.* (2013), natural abundance  $\text{SO}_2$  of Franz *et al.* (2013), S<sup>0</sup>-1 and S<sup>0</sup>-2 of Whitehill *et al.* (2015), D2 experiments of Endo *et al.* (2016), and all of Endo *et al.* (2019). Note that we did not consider differences between UV light sources or differences born out of photolysis spectral range (cross-section in this report is from 206 to 220 nm).

ted for comparison with this study. Although some differences exist between spectral resolution and pressure broadened spectra, Fig. 7 shows the slopes of fractionation factors/column density with respect to the  $\text{SO}_2$  absorption line width at a constant  $\text{SO}_2$  column density. The absorption line width was assumed to be  $1 \text{ cm}^{-1}$ ,

which is equal to the spectral resolution. Meanwhile, the line widths were estimated from pressure broadening, namely, the total atmospheric pressures and a pressure broadening coefficient of  $\text{SO}_2$  ( $0.30 \pm 0.03 \text{ cm}^{-1} \text{ atm}^{-1}$  for  $\text{N}_2$  atmosphere, Lyons *et al.*, 2018).

In the photolysis experiments conducted by Endo *et*

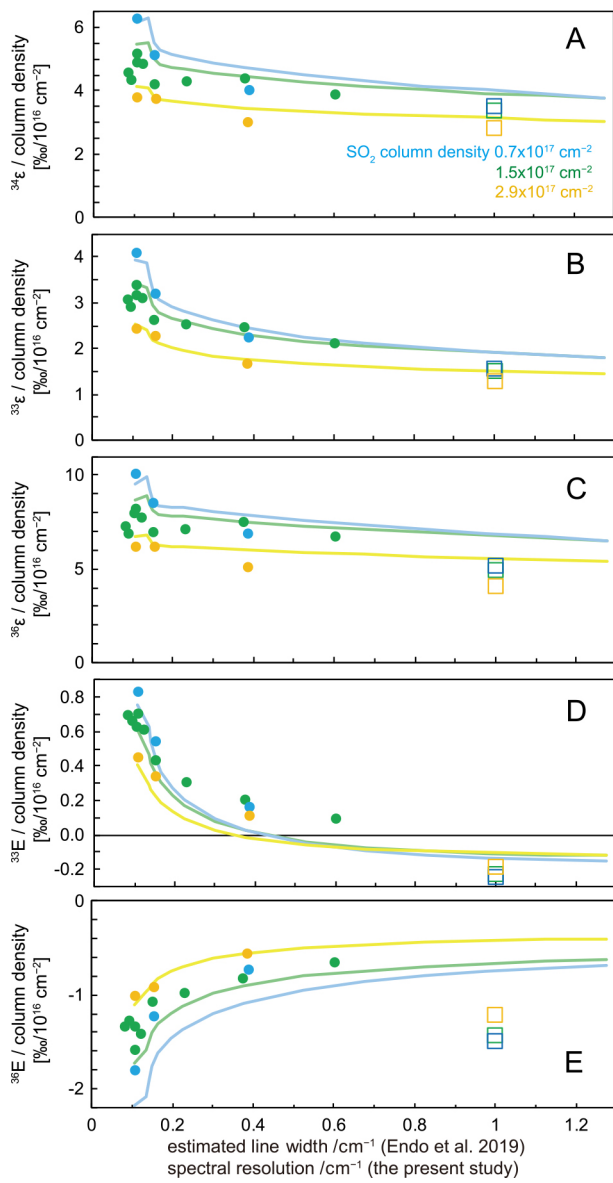


**Fig. 7.** Relationships between slopes of isotope fractionations/  $\text{SO}_2$  column density (that is, (A)  ${}^{34}\epsilon/\text{SO}_2$  column density, (B)  ${}^{33}\epsilon/\text{SO}_2$  column density, (C)  ${}^{36}\epsilon/\text{SO}_2$  column density, (D)  ${}^{33}E/\text{SO}_2$  column density, and (E)  ${}^{36}E/\text{SO}_2$  column density) and  $\text{SO}_2$  absorption line width or spectral resolution at fixed  $\text{SO}_2$  column density. Colors represent  $\text{SO}_2$  column density. Squares represent this study whereas circles represent previous photolysis experiments (Endo *et al.*, 2019). Lines are calculated by revised cross-sections from Endo *et al.* (2019). The y-axes represent “slopes”, so that fractionation factors at each  $\text{SO}_2$  column density subtracted by those at optically thin  $\text{SO}_2$  (i.e., an  $\text{SO}_2$  column density of  $0 \text{ cm}^{-2}$ ) were divided by  $\text{SO}_2$  column densities. For the slopes of Endo *et al.* (2019), fractionation factors of “D2 0 Pa (estimate)” in Endo *et al.* (2016) were used as the fractionation factors at the optically thin  $\text{SO}_2$ .

*al.* (2019), the total pressure dependence of the  ${}^{34}\epsilon/\text{SO}_2$  column density was relatively small, suggesting that the absorption line width does not strongly affect  ${}^{34}\epsilon$  (Fig. 7A). This is consistent with the fact that this study ( $\sim 1 \text{ cm}^{-1}$ ) reproduced the  ${}^{34}\epsilon/\text{column density}$  of photoly-

sis experiments, despite the unresolved absorption spectra (Fig. 6A and B). On the other hand, this study’s predicted negative  ${}^{33}E/\text{SO}_2$  column density did not match the results of previous experiments (Fig. 6G and H). However, the  ${}^{33}E/\text{column density}$  slope was sensitive to the total pressure and clearly decreased at high total pressure (Fig. 7D). At  $>0.5 \text{ cm}^{-1}$  of the estimated  $\text{SO}_2$  absorption line width, a negative  ${}^{33}E/\text{column density}$  was predicted (Fig. 7D, lines), which was consistent with the results of this study. With regards to  ${}^{33}\epsilon$  and  ${}^{36}\epsilon$ , the relationship between the  $\text{SO}_2$  column density (Fig. 6C–F) and absorption line width (Fig. 7B and C) displayed similarities to the  ${}^{34}\epsilon$  trends; however, they are not as easily reproducible as  ${}^{34}\epsilon$ . With regard to  ${}^{36}E$ , this study reproduced results within an approximately 10% variation below  $5 \times 10^{17} \text{ cm}^2$ . However, the  ${}^{36}E/\text{SO}_2$  column density slope did not reproduce the broadening model well (Fig. 7E). Consequently,  ${}^{32,33,34,36}\text{SO}_2$  cross-sections may also reproduce  ${}^{33}E/\text{column density}$  when the spectral resolution is improved; however, this is a topic requiring further research. At  $>10^{18} \text{ cm}^{-2}$  of  $\text{SO}_2$  column density, the  ${}^{34}\epsilon$  in this study is overestimated in comparison to that of photochemical experiments (Fig. 6A). The cause for this is ultimately unclear; however, if a gas with broad absorption spectra exists, the  $\text{SO}_2$  photolysis rate will decrease at the rear side of the chamber, and the observed fractionations will be smaller than the predicted fractionations of the column density.

Taken together, the  ${}^{32,33,34,36}\text{SO}_2$  absorption spectra reported by this study are likely useful for predicting  ${}^{34}\epsilon$  during  $\text{SO}_2$  photolysis at below  $10^{18} \text{ cm}^{-2}$  of  $\text{SO}_2$  column density. The spectral resolution dependence of the  ${}^{34}\epsilon/\text{SO}_2$  column density is small, and  ${}^{34}\epsilon/\text{SO}_2$  column density of Endo *et al.* (2015) is similar to that of this study (Fig. 5A). Endo *et al.* (2015) may be more convenient to utilize than this study, given the availability of 190–220-nm wavelength cross-sections, enhanced precision, and relative ease of calculation due to its low spectral resolution and coarse wavelength steps. Since  ${}^{33}E$  is sensitive to the  $\text{SO}_2$  absorption line width, this study could not predict  ${}^{33}E$  at less than  $\sim 1$  bar atmospheric pressure, where the absorption line width is less than  $\sim 0.3 \text{ cm}^{-1}$  (Fig. 7D). On the contrary, at high atmospheric pressures in which the absorption line width reaches  $\sim 1 \text{ cm}^{-1}$ , such as in the Venus’ atmosphere, it may be possible to predict  ${}^{33}E$  (Fig. 7D).

#### Applying a self-shielding model using the synthesized absorption spectra to laboratory experiments and natural samples

As described in Section “Calculations of self-shielding using synthesized absorption spectra”, in the case of complete discrete absorption spectra of  $\text{SO}_2$  (Fig. 1A), the self-shielding during  $\text{SO}_2$  photolysis arises from MIF-S with  ${}^{33}E/{}^{34}\epsilon$  and  ${}^{36}E/{}^{33}E$  of +0.52 and -1.63,

respectively. Interestingly, the slopes are closer to the Archean MIF-S ( $\Delta^{33}\text{S}/\delta^{34}\text{S} \sim +0.9$ ,  $\Delta^{36}\text{S}/\Delta^{33}\text{S} \sim -0.9$ ), than the MIF-S as predicted by the  $\text{SO}_2$  cross-section of this study ( $\Delta^{33}\text{S}/\delta^{34}\text{S} \sim -0.1$ , positive  $\Delta^{36}\text{S}/\Delta^{33}\text{S}$ ) and as observed in  $\text{SO}_2$  photolysis experiments ( $\Delta^{33}\text{S}/\delta^{34}\text{S} \leq \sim +0.1$ ,  $\Delta^{36}\text{S}/\Delta^{33}\text{S} \leq \sim -2.4$ ). The observation that the slopes are different from the ideally discrete spectra case implies that the absorption spectra of  ${}^{32}\text{SO}_2$  overlap with those of  ${}^{33}\text{SO}_2$ ; that is, UV attenuation by  ${}^{32}\text{SO}_2$  absorption decreases not only the  ${}^{32}\text{SO}_2$  photolysis rate constants but also the  ${}^{33}\text{SO}_2$  photolysis rate constants (e.g., Ono, 2017; Endo *et al.*, 2019; Lyons, 2020). Isotope fractionation by self-shielding under the ideal conditions in which absorption lines are narrow can be tested with further laboratory experiments such as  $\text{SO}_2$  photolysis at low temperature and low pressure and photolysis using a species with a more discrete absorption spectra (e.g., sulfur monoxide (SO), Sarka and Nanbu, 2019).

This simple model predicted that self-shielding leads to large clumped isotope depletion in products and enrichment in reagents (Section “Calculations of self-shielding using synthesized absorption spectra”). Clumped isotopes may possibly be a fingerprint of self-shielding. However, signatures related to self-shielding have not been identified. In the case of  $\text{SO}_2$  photolysis, S–O clumped isotopes are enriched in residual  $\text{SO}_2$  and are depleted in the product SO. To preserve the clumped isotope signatures, S–O bonds must remain in the molecules. In laboratory experiments of  $\text{SO}_2$  photolysis (e.g., Ono *et al.*, 2013), the S–O bonds in the residual  $\text{SO}_2$  would remain, although the bonds in the produced SO were likely destroyed via SO photolysis. Therefore, an enrichment signature may exist in residual  $\text{SO}_2$ . However, thus far, methods for analyzing S–O clumped isotopes in  $\text{SO}_2$  have not been developed; it follows that, to test this, sufficient analysis methods must be developed.

## Conclusions

We measured the  ${}^{32}\text{SO}_2$ ,  ${}^{33}\text{SO}_2$ ,  ${}^{34}\text{SO}_2$ , and  ${}^{36}\text{SO}_2$  absorption spectra from 206 to 220 nm at 296 K, set to  $1\text{ cm}^{-1}$  wavelength resolution. The resolution was 25 times higher than has been previously reported. The accuracy was approximately 10%. Compared with previous reports of high-resolution spectra for  $\text{SO}_2$  at natural abundance, the wavelength appeared to offset from  $\sim 0.016$  nm, and the magnitudes of the cross-section at the absorption peak wavelength seemed small. However, this had insignificant effects on modeling isotopic self-shielding. Using the measured absorption spectra, we estimated the sulfur isotope fractionation by self-shielding in  $\text{SO}_2$  photolysis.

This study roughly reproduced the  ${}^{34}\varepsilon/(\text{SO}_2 \text{ column density})$  slope of previous  $\text{SO}_2$  photolysis experiments; however, the spectral resolution was insufficient to

resolve the Doppler widths. This finding likely reflects the insensitivity of  ${}^{34}\varepsilon$  to the absorption line width, which is supported by the total pressure effect observed in previous  $\text{SO}_2$  photolysis experiments. The second key characteristic of the prediction was the negative  ${}^{33}\text{E}/(\text{SO}_2 \text{ column density})$  slope. This did not match previous photolysis experiments, but was consistent with prior observations that the slopes were smaller in  $\text{SO}_2$  photolysis experiments at higher total pressures. Under a high  $p\text{SO}_2$  atmosphere, strong self-shielding and strong pressure broadening should occur. This provides the basis for the novel suggestion that spectroscopic research may be linked to photolysis experiments with MIF-S.

Additionally, we modeled an ideal case in which the absorption lines are narrow below the Doppler width. The produced self-shielding originates from MIF-S closer to the Archean trend than described in previous photolysis experiments and spectroscopic measurements. This suggests that self-shielding remains a major candidate for MIF-S in the Archean atmosphere.

**Acknowledgments** We would like to thank Shohei Hattori and Naohiro Yoshida for sample preparation and Matthew S. Johnson for technical advice. We also thank James Lyons and an anonymous reviewer for their constructive comments. The editor, Tsubasa Otake, provided advice on the organization of the paper. Cross-sections of  ${}^{32,33,34,36}\text{SO}_2$  reported by Lyons (2007) were provided by James Lyons. This research was funded by JSPS KAKENHI (grant numbers JP16J06990, JP17H06105, JP20H01975, JP20K14593, and 24740364). The authors would also like to thank Editage (www.editage.com) for English language editing.

## References

- Avic, G., Marty, B., Burgess, R., Hofmann, A., Philippot, P., Zahnle, K. and Zakharov, D. (2018) Evolution of atmospheric xenon and other noble gases inferred from Archean to Paleoproterozoic rocks. *Geochim. Cosmochim. Acta* **232**, 82–100.
- Babikov, D. (2017) Recombination reactions as a possible mechanism of mass-independent fractionation of sulfur isotopes in the Archean atmosphere of Earth. *Proc. Natl Acad. Sci. USA* **114**, 3062–3067.
- Ball, C. D., Dutta, J. M., Goyette, T. M., Helmlinger, P. and De Lucia, F. C. (1996) The pressure broadening of  $\text{SO}_2$  by  $\text{N}_2$ ,  $\text{O}_2$ , He, and  $\text{H}_2$  between 90 and 500 K. *J. Quant. Spectrosc. Radiat Transf.* **56**, 109–117.
- Blackie, D., Blackwell-Whitehead, R., Stark, G., Pickering, J. C., Smith, P. L., Rufus, J. and Thorne, A. P. (2011) High-resolution photoabsorption cross-section measurements of  $\text{SO}_2$  at 198 K from 213 to 325 nm. *J. Geophys. Res.* **116**, E03006.
- Cazzoli, G. and Puzzarini, C. (2012)  $\text{N}_2^-$ ,  $\text{O}_2^-$ ,  $\text{H}_2^-$ , and He-broadening of  $\text{SO}_2$  rotational lines in the mm-/submm-wave and THz frequency regions: The  $J$  and  $K_a$  dependence. *J. Quant. Spectrosc. Radiat. Transf.* **113**, 1051–1057.
- Chakraborty, S., Ahmed, M., Jackson, T. L. and Thiemens, M. H. (2008) Experimental test of self-shielding in vacuum ultraviolet photodissociation of CO. *Science* **321**, 1328–1331.
- Chakraborty, S., Muskatel, B. H., Jackson, T. L., Ahmed, M., Levine,

- R. D. and Thiemens, M. H. (2014) Massive isotopic effect in vacuum UV photodissociation of N<sub>2</sub> and implications for meteorite data. *Proc. Natl. Acad. Sci. USA* **111**, 14704–14709.
- Claire, M. W., Kasting, J. F., Domagal-Goldman, S. D., Stüeken, E. E., Buick, R. and Meadows, V. S. (2014) Modeling the signature of sulfur mass-independent fractionation produced in the Archean atmosphere. *Geochim. Cosmochim. Acta* **141**, 365–380.
- Danielache, S. O., Eskebjerg, C., Johnson, M. S., Ueno, Y. and Yoshida, N. (2008) High-precision spectroscopy of <sup>32</sup>S, <sup>33</sup>S, and <sup>34</sup>S sulfur dioxide: Ultraviolet absorption cross sections and isotope effects. *J. Geophys. Res.* **113**, D17314.
- Danielache, S. O., Hattori, S., Johnson, M. S., Ueno, Y., Nanbu, S. and Yoshida, N. (2012) Photoabsorption cross-section measurements of <sup>32</sup>S, <sup>33</sup>S, <sup>34</sup>S, and <sup>36</sup>S sulfur dioxide for the B<sup>1</sup>B<sub>1</sub>-X<sup>1</sup>A<sub>1</sub> absorption band. *J. Geophys. Res.* **117**, D24301.
- Eiler, J. M. (2007) “Clumped-isotope” geochemistry—The study of naturally-occurring, multiply-substituted isotopologues. *Earth Planet. Sci. Lett.* **262**, 309–327.
- Endo, Y., Danielache, S. O., Ueno, Y., Hattori, S., Johnson, M. S., Yoshida, N. and Kjaergaard, H. G. (2015) Photoabsorption cross-section measurements of <sup>32</sup>S, <sup>33</sup>S, <sup>34</sup>S, and <sup>36</sup>S sulfur dioxide from 190 to 220 nm. *J. Geophys. Res. Atmos.* **120**, 2546–2557.
- Endo, Y., Ueno, Y., Aoyama, S. and Danielache, S. O. (2016) Sulfur isotope fractionation by broadband UV radiation to optically thin SO<sub>2</sub> under reducing atmosphere. *Earth Planet. Sci. Lett.* **453**, 9–22.
- Endo, Y., Danielache, S. O. and Ueno, Y. (2019) Total pressure dependence of sulfur mass-independent fractionation by SO<sub>2</sub> photolysis. *Geophys. Res. Lett.* **46**, 483–491.
- Farquhar, J. (2018) Sulfur Isotopes. *Encyclopedia of Geochemistry. Encyclopedia of Earth Sciences Series* (White M. W. ed.), Springer, Cham. [https://doi.org/10.1007/978-3-319-39193-9\\_74-1](https://doi.org/10.1007/978-3-319-39193-9_74-1)
- Farquhar, J., Bao, H. and Thiemens, M. (2000a) Atmospheric influence of Earth’s earliest sulfur cycle. *Science* **289**, 756–759.
- Farquhar, J., Savarino, J., Jackson, T. L. and Thiemens, M. H. (2000b) Evidence of atmospheric sulphur in the martian regolith from sulphur isotopes in meteorites. *Nature* **404**, 50–52.
- Farquhar, J., Savarino, J., Airieau, S. and Thiemens, M. H. (2001) Observation of wavelength-sensitive mass-independent sulfur isotope effects during SO<sub>2</sub> photolysis: Implications for the early atmosphere. *J. Geophys. Res.* **106**, 32829–32839.
- Feaga, L. M., McGrath, M. and Feldman, P. D. (2009) Io’s dayside SO<sub>2</sub> atmosphere. *Icarus* **201**, 570–584.
- Franz, H. B., Danielache, S. O., Farquhar, J. and Wing, B. A. (2013) Mass-independent fractionation of sulfur isotopes during broadband SO<sub>2</sub> photolysis: Comparison between <sup>16</sup>O- and <sup>18</sup>O-rich SO<sub>2</sub>. *Chem. Geol.* **362**, 56–65.
- Freeman, D. E., Yoshino, K., Esmond, J. R., and Parkinson, W. H. (1984) High resolution absorption cross section measurements of SO<sub>2</sub> at 213 K in the wavelength region 172–240 nm. *Planet. Space Sci.* **32**, 1125–1134.
- Gaillard, F., Scaillet, B. and Arndt, N. T. (2011) Atmospheric oxygenation caused by a change in volcanic degassing pressure. *Nature* **478**, 229–232.
- Gordon, I. E., Rothman, L. S., Hill, C., Kochanov, R. V., Tan, Y., Bernath, P. F., Birk, M., Boudon, V., Campargue, A., Chance, K. V., Drouin, B. J., Flaud, J. -M., Gamache, R. R., Hodges, J. T., Jacquemart, D., Perevalov, V. I., Perrin, A., Shine, K. P., Smith, M. -A. H., Tennyson, J., Toon, G. C., Tran, H., Tyuterev, V. G., Barbe, A., Császár, A. G., Devi, V. M., Furtenbacher, T., Harrison, J. J., Hartmann, J. -M., Jolly, A., Johnson, T. J., Karman, T., Kleiner, I., Kyuberis, A. A., Loos, J., Lyulin, O. M., Massie, S. T., Mikhailenko, S. N., Moazzen-Ahmadi, N., Müller, H. S. P., Naumenko, O. V., Nikitin, A. V., Polyansky, O. L., Rey, M., Rotger, M., Sharpe, S. W., Sung, K., Starikova, E., Tashkun, S. A., Auwera, J. V., Wagner, G., Wilzewski, J., Wcislo, P., Yu, S. and Zak, E. J. (2017) The HITRAN2016 molecular spectroscopic database. *J. Quant. Spectrosc. Radiat. Transf.* **203**, 3–69.
- Halevy, I., Zuber, M. T. and Schrag, D. P. (2007) A sulfur dioxide climate feedback on early Mars. *Science* **318**, 1903–1907.
- Harris, E., Sinha, B., Hoppe, P., Crowley, J. N., Ono, S. and Foley, S. (2012) Sulfur isotope fractionation during oxidation of sulfur dioxide: gas-phase oxidation by OH radicals and aqueous oxidation by H<sub>2</sub>O<sub>2</sub>, O<sub>3</sub> and iron catalysis. *Atmos. Chem. Phys.* **12**, 407–423.
- Harman, C. E., Pavlov, A. A., Babikov, D. and Kasting, J. F. (2018) Chain formation as a mechanism for mass-independent fractionation of sulfur isotopes in the Archean atmosphere. *Earth Planet. Sci. Lett.* **496**, 238–247.
- Heicklen, J., Kelly, N. and Partymiller, K. (1980) The photophysics and photochemistry of SO<sub>2</sub>. *Rev. Chem. Intermed.* **3**, 315–404.
- Hermans, C., Vandaele, A. C. and Fally, S. (2009) Fourier transform measurements of SO<sub>2</sub> absorption cross sections: I. Temperature dependence in the 24 000–29 000 cm<sup>-1</sup> (345–420 nm) region, *J. Quant. Spectrosc. Radiat. Transf.* **110**, 756–765.
- Holland, H. D. (2002) Volcanic gases, black smokers, and the great oxidation event. *Geochim. Cosmochim. Acta* **66**, 3811–3826.
- Ignatiev, A. V., Velivetskaya, T. A. and Yakovenko, V. V. (2019) Effect of mass-independent isotope fractionation of sulfur ( $\Delta^{33}\text{S}$  and  $\Delta^{36}\text{S}$ ) during SO<sub>2</sub> photolysis in experiments with a broadband light source. *Geochemistry Int.* **57**, 751–760.
- Izon, G., Zerkle, A. L., Williford, K. H., Farquhar, J., Poulton, S. W. and Claire, M. W. (2017) Biological regulation of atmospheric chemistry en route to planetary oxygenation. *Proc. Natl. Acad. Sci. USA* **114**, E2571–E2579.
- Johnson, S. S., Mischna, M. A., Grove, T. L. and Zuber, M. T. (2008) Sulfur-induced greenhouse warming on early Mars. *J. Geophys. Res.* **113**, E08005.
- Katagiri, H., Sako, T., Hishikawa, A., Yazaki, T., Onda, K., Yamanouchi, K. and Yoshino, K. (1997) Experimental and theoretical exploration of photodissociation of SO<sub>2</sub> via the <sup>1</sup>B<sub>2</sub> state: identification of the dissociation pathway. *J. Mol. Struct.* **413–414**, 589–614.
- Koplow, J. P., Kliner, D. A. V. and Goldberg, L. (1998) Development of a narrow-band, tunable, frequency-quadrupled diode laser for UV absorption spectroscopy. *Appl. Opt.* **37**, 3954–3960.
- Kroll, J. A., Frandsen, B. N., Rapf, R. J., Kjaergaard, H. G. and Vaida, V. (2018) Reactivity of electronically excited SO<sub>2</sub> with alkanes. *J. Phys. Chem. A* **122**, 7782–7789.
- Kühnemann, F., Heiner, Y., Sumpf, B. and Herrmann, Ka. (1992) Line broadening in the v<sub>3</sub> band of SO<sub>2</sub>: Studied with diode laser spectroscopy. *J. Mol. Spectrosc.* **152**, 1–12.
- Lin, M. and Thiemens, M. H. (2020) A simple elemental sulfur reduction method for isotopic analysis and pilot experimental tests of symmetry-dependent sulfur isotope effects in planetary processes. *Geochim. Geophys. Geosyst.* **21**, e2020GC009051.
- Lyons, J. R. (2007) Mass-independent fractionation of sulfur isotopes by isotope-selective photodissociation of SO<sub>2</sub>. *Geophys. Res. Lett.* **34**, L22811.
- Lyons, J. R. (2020) An analytical formulation of isotope fractionation

- due to self-shielding. *Geochim. Cosmochim. Acta* **282**, 177–200.
- Lyons, J. R., Herde, H., Stark, G., Blackie, D. S., Pickering, J. C. and de Oliveira, N. (2018) VUV pressure-broadening in sulfur dioxide. *J. Quant. Spectrosc. Radiat. Transf.* **210**, 156–164.
- Masterson, A. L., Farquhar, J. and Wing, B. A. (2011) Sulfur mass-independent fractionation patterns in the broadband UV photolysis of sulfur dioxide: Pressure and third body effects. *Earth Planet. Sci. Lett.* **306**, 253–260.
- Miller, C. E. and Yung, Y. L. (2000) Photo-induced isotopic fractionation. *J. Geophys. Res.* **105**, 29039–29051.
- Mishima, K., Yamazaki, R., Satish-Kumar, M., Ueno, Y., Hokada, T. and Toyoshima, T. (2017) Multiple sulfur isotope geochemistry of Dharwar Supergroup, Southern India: Late Archean record of changing atmospheric chemistry. *Earth Planet. Sci. Lett.* **464**, 69–83.
- Ohmoto, H. (2020) A seawater-sulfate origin for early Earth's volcanic sulfur. *Nature Geosci.* **13**, 576–583.
- Okabe, H. (1971) Fluorescence and predissociation of sulfur dioxide. *J. Am. Chem. Soc.* **93**, 7095–7096.
- Olson, S. L., Ostrander, C. M., Gregory, D. D., Roy, M., Anbar, A. D. and Lyons, T. W. (2019) Volcanically modulated pyrite burial and ocean–atmosphere oxidation. *Earth Planet. Sci. Lett.* **506**, 417–427.
- Okazaki, A., Ebata, T., and Mikami, N. (1997) Degenerate four-wave mixing and photofragment yield spectroscopic study of jet-cooled SO<sub>2</sub> in the C<sup>1</sup>B<sub>2</sub> state: Internal conversion followed by dissociation in the X state. *J. Chem. Phys.* **107**, 8752–8758.
- Ono, S. (2017) Photochemistry of sulfur dioxide and the origin of mass-independent isotope fractionation in Earth's atmosphere. *Annu. Rev. Earth Planet. Sci.* **45**, 301–329.
- Ono, S., Kaufman, A. J., Farquhar, J., Sumner, D. Y. and Beukes, N. J. (2009) Lithofacies control on multiple-sulfur isotope records and Neoarchean sulfur cycles. *Precambrian Res.* **169**, 58–67.
- Ono, S., Whitehill, A. R. and Lyons, J. R. (2013) Contribution of isotopeologue self-shielding to sulfur mass-independent fractionation during sulfur dioxide photolysis. *J. Geophys. Res. Atmos.* **118**, 2444–2454.
- Pavlov, A. A. and Kasting, J. F. (2002) Mass-independent fractionation of sulfur isotopes in Archean sediments: Strong evidence for an anoxic Archean atmosphere. *Astrobiology* **2**, 27–41.
- Ran, H., Xie, D. and Guo, H. (2007) Theoretical studies of equation C<sup>1</sup>B<sub>2</sub> absorption spectra of SO<sub>2</sub> isotopomers. *Chem. Phys. Lett.* **439**, 280–283.
- Romero, A. B. and Thiemens, M. H. (2003) Mass-independent sulfur isotopic compositions in present-day sulfate aerosols. *J. Geophys. Res. Atmos.* **108**, 4524.
- Rufus, J., Stark, G., Smith, P. L., Pickering, J. C. and Thorne, A. P. (2003) High-resolution photoabsorption cross-section measurements of SO<sub>2</sub>, 2: 220 to 325 nm at 295 K. *J. Geophys. Res.* **108**, 5011.
- Rufus, J., Stark, G., Thorne, A. P., Pickering, J. C., Blackwell-Whitehead, R. J., Blackie, D. and Smith, P.L. (2009) High-resolution photoabsorption cross-section measurements of SO<sub>2</sub> at 160 K between 199 and 220 nm. *J. Geophys. Res.* **114**, E06003.
- Sarka, K. and Nanbu, S. (2019) Total absorption cross section for UV excitation of sulfur monoxide. *J. Phys. Chem. A* **123**, 3697–3702.
- Savarino, J., Romero, A., Cole-Dai, J., Bekki, S. and Thiemens, M. H. (2003) UV induced mass-independent sulfur isotope fractionation in stratospheric volcanic sulfate. *Geophys. Res. Lett.* **30**, 2131.
- Stark, G., Smith, P. L., Rufus, J., Thorne, A. P., Pickering, J. C. and Cox, G. (1999) High-resolution photoabsorption cross-section measurements of SO<sub>2</sub> at 295 K between 198 and 220 nm. *J. Geophys. Res.* **104**, 16585–16590.
- Sumpf, B., Fleischmann, O. and Kronfeldt, H. -D. (1996a) Self-, air-, and nitrogen-broadening in the v<sub>1</sub> band of SO<sub>2</sub>. *J. Mol. Spectrosc.* **176**, 127–132.
- Sumpf, B., Schöne, M. and Kronfeldt, H. -D. (1996b) Self- and air-broadening in the v<sub>3</sub> band of SO<sub>2</sub>. *J. Mol. Spectrosc.* **179**, 137–141.
- Sumpf, B. (1997) Experimental investigation of the self-broadening coefficients in the v<sub>1</sub> + v<sub>3</sub> band of SO<sub>2</sub> and the 2v<sub>2</sub> band of H<sub>2</sub>S. *J. Mol. Spectrosc.* **181**, 160–167.
- Tasinato, N., Charmet, A. P., Stoppa, P., Giorgianni, S. and Buffa, G. (2010) Spectroscopic measurements of SO<sub>2</sub> line parameters in the 9.2 μm atmospheric region and theoretical determination of self-broadening coefficients. *J. Chem. Phys.* **132**, 044315.
- Tasinato, N., Charmet, A. P., Stoppa, P., Buffa, G. and Puzzarini, C. (2013) A complete listing of sulfur dioxide self-broadening coefficients for atmospheric applications by coupling infrared and microwave spectroscopy to semiclassical calculations. *J. Quant. Spectrosc. Radiat. Transf.* **130**, 233–248.
- Tasinato, N., Charmet, A. P., Stoppa, P., Giorgianni, S. and Buffa, G. (2014) N<sub>2</sub>-, O<sub>2</sub>-and He-collision-induced broadening of sulfur dioxide ro-vibrational lines in the 9.2 μm atmospheric window. *Spectrochim. Acta A* **118**, 373–379.
- Thiemens, M. H. and Lin, M. (2021) Discoveries of mass independent isotope effects in the solar system: Past, present and future. *Rev. Mineral. Geochem.* **86**, 35–95.
- Tokue, I. and Nanbu, S. (2010) Theoretical studies of absorption cross sections for the C<sup>1</sup>B<sub>2</sub>-X<sup>1</sup>A<sub>1</sub> system of sulfur dioxide and isotope effects. *J. Chem. Phys.* **132**, 024301.
- Ueno, Y., Johnson, M. S., Danielache, S. O., Eskebjerg, C., Pandey, A. and Yoshida, N. (2009) Geological sulfur isotopes indicate elevated OCS in the Archean atmosphere, solving faint young sun paradox. *Proc. Natl. Acad. Sci. USA* **106**, 14784–14789.
- Vandaele, A. C., Simon, P. C., Guilmot, J. M., Carleer, M. and Colin, R. (1994) SO<sub>2</sub> absorption cross section measuring in the UV using a Fourier transform spectrometer. *J. Geophys. Res. Atoms.* **99**, 25599–25605.
- Vandaele, A. C., Hermans, C. and Fally, S. (2009) Fourier transform measurements of SO<sub>2</sub> absorption cross sections: II. Temperature dependence in the 29 000–44 000 cm<sup>-1</sup> (227–345 nm) region. *J. Quant. Spectrosc. Radiat. Transf.* **110**, 2115–2126.
- Vandaele, A. C., Koralev, O., Belyaev, D., Chamberlain, S., Evdokimova, D., Encrenaz, Th., Esposito, L., Jessup, K. L., Lefèvre, F., Limaye, S., Mahieux, A., Marcq, E., Mills, F. P., Montmessin, F., Parkinson, C. D., Robert, S., Roman, T., Sandor, B., Stolzenbach, A., Wilson, C. and Wilquet, V. (2017) Sulfur dioxide in the Venus atmosphere: I. Vertical distribution and variability. *Icarus* **295**, 16–33.
- Wang, D. T., Welander, P. V. and Ono, S. (2016) Fractionation of the methane isotopologues <sup>13</sup>CH<sub>4</sub>, <sup>12</sup>CH<sub>3</sub>D, and <sup>13</sup>CH<sub>3</sub>D during aerobic oxidation of methane by *Methylococcus capsulatus* (Bath). *Geochim. Cosmochim. Acta* **192**, 186–202.
- Whitehill, A. R. and Ono, S. (2012) Excitation band dependence of sulfur isotope mass-independent fractionation during photochemistry of sulfur dioxide using broadband light sources. *Geochim. Cosmochim. Acta* **94**, 238–253.
- Whitehill, A. R., Xie, C., Hu, X., Xie, D., Guo, H. and Ono, S. (2013)

- Vibronic origin of sulfur mass-independent isotope effect in photo-excitation of SO<sub>2</sub> and the implications to the early Earth's atmosphere. *Proc. Natl. Acad. Sci. USA* **110**, 17697–17702.
- Whitehill, A. R., Jiang, B., Guo, H. and Ono, S. (2015) SO<sub>2</sub> photolysis as a source for sulfur mass-independent isotope signatures in stratospheric aerosols. *Atmos. Chem. Phys.* **15**, 1843–1864.
- Whitehill, A. R., Joelsson, L. M. T., Schmidt, J. A., Wang, D. T., Johnson, M. S. and Ono, S. (2017) Clumped isotope effects during OH and Cl oxidation of methane. *Geochim. Cosmochim. Acta* **196**, 307–325.
- Wu, C. Y. R., Yang, B. W., Chen, F. Z., Judge, D. L., Caldwell, J. and Trafton, L. M. (2000) Measurements of high-, room-, and low-temperature photoabsorption cross sections of SO<sub>2</sub> in the 2080- to 2950-Å region, with application to Io. *Icarus* **145**, 289–296.
- Yeung, L. Y., Li, S., Kohl, I. E., Haslun, J. A., Ostrom, N. E., Hu, H., Fischer, T. P., Schauble, E. A. and Young, E. D. (2017) Extreme enrichment in atmospheric <sup>15</sup>N/<sup>14</sup>N. *Sci. Adv.* **3**, eaao6741.
- Zahnle, K., Claire, M. and Catling, D. (2006) The loss of mass-independent fractionation in sulfur due to a Palaeoproterozoic collapse of atmospheric methane. *Geobiology* **4**, 271–283.
- Zahnle, K. J., Gacesa, M. and Catling, D. C. (2019) Strange messenger: A new history of hydrogen on Earth, as told by Xenon. *Geochim. Cosmochim. Acta* **244**, 56–85.
- Zerkle, A. L., Claire, M. W., Domagal-Goldman, S. D., Farquhar, J. and Poulton, S. W. (2012) A bistable organic-rich atmosphere on the Neoarchean Earth. *Nat. Geosci.* **5**, 359–363.

#### Supplementary Materials

[https://www.jstage.jst.go.jp/article/geochemj/56/1/56\\_GJ22004/\\_article](https://www.jstage.jst.go.jp/article/geochemj/56/1/56_GJ22004/_article)

- Supporting text 1–2
- Figures S1–S6
- Table (CSV file)